Study of the precipitation characteristics around mountainous regions in South Asia and South America

Dibas Shrestha

A dissertation for the degree of Doctor of Science

Department of Earth and Environmental Sciences,

Graduate School of Environmental Studies,

Nagoya University

2012

Abstract

Precipitation characteristics and circulation, specifically focusing on its relationship with elevation, are examined over mountainous regions of South Asia and South America utilizing the Tropical Rainfall Measuring Mission (TRMM) Precipitation Radar (PR) data, the Japanese 25-year Reanalysis (JRA-25), and the Global 30 Arc-Second Elevation Data Set (GTOPO30). This study presents a comparative analysis of precipitation mechanisms over the rugged topography under moist and rather dry atmospheric conditions.

First, the rainfall-elevation relationship in the central Himalayan region (CHR) for pre-monsoon and monsoon seasons is analyzed using the 11-year (1998–2008) TRMM PR data of spatial resolution 0.1° × 0.1° (approximately 10 × 10 km). Furthermore, variability of precipitation characteristics is studied for Himalayan active and break periods. The TRMM product 3B42 is used for the identification of active and break periods. The results indicate a large-scale relationship between rainfall and elevation during both seasons. The investigation reveals a relatively large amount of rainfall over higher elevations during pre-monsoon season. During summer monsoon, there appear well known double peaks of rainfall over the southern slope of the Himalayas. The first primary peak appears along the Sub-Himalayas (~500–700 m above MSL), while the second appears along the Lesser Himalayas (~2,000–2,200 m above MSL). The former rainfall peak is attributed to fewer heavy rainfall events, and the latter to frequent, weak, but persistent rainfall. It is suggested that the atmosphere is insufficiently moist to trigger convections during the pre-monsoon season, and sufficiently moist during summer monsoon season. The convections over the Sub-Himalayas may moisten the middle layer, and the water vapor in the atmosphere condenses because of the forced lifting along the slope,

forming the second rainfall band. The total rain amount is primarily determined by the frequency of rain. The rain-conditioned rain rate along the slope monotonically decreases with elevation. This shows that the precipitation occurs because of forced lifting. In addition, our results show that seasonal variation of rainfall is rather similar to the variation of rainfall characteristics observed during active and break periods.

Next, we focus our analysis around the coastal mountains: Western Ghats (WG), and the Myanmar Western Coast (MWC). The high spatial resolution (0.05° × 0.05°) TRMM PR data sets are investigated for 1998–2010 to characterize the summer precipitation. In the both WG and MWC, maximum rainfall along a tight line on the upwind side of the coastal mountains is primarily attributed to rain frequency. However, intense precipitation was observed over the offshore regions. Compared with the WG, deeper and large-scale precipitation systems develop over the MWC regions, producing more-intense rainfall. It is suggested that insufficient humidity deters large-scale convection over the WG, and the atmosphere is sufficiently moist over the MWC regions.

Over the Andes, the zone of rainfall maxima observed over the higher terrain of the central and southern regions is attributed to rainfall frequency and intensity, respectively. In the foothills of the central Andes, a persistent rain system occurs when moist low-level flow is lifted. In contrast, a relatively dry atmosphere and steep mountain slopes favor deep convection in the southern Andes foothills.

Overall, this study indicates distinct precipitation mechanisms over the complex mountain terrain in more and less humid atmospheric conditions. When atmosphere is sufficiently humid, wide area precipitation systems are easily triggers over the foothills under

relatively stable atmospheric conditions. Thus, large amount of rainfall occurs over the low-altitude areas and decreases with altitude. On the other hand, atmosphere is rather unstable under less humid atmospheric conditions, resulting intense rainfall over a certain altitude. Although further quantitative and qualitative investigations are needed to clarify these results, this study emphasizes that low-level moisture condition is a key component to determine the precipitation mechanisms around the mountainous regions.

Contents

1. Introduction

1.1 Background of study

Orographic response to the atmosphere is one of the most influential factors affecting spatial and temporal distribution of precipitation around mountainous areas, because mountains alter the flow of air and respond to solar radiation differently than the surrounding atmosphere [*Barros and Lettenmaier*, 1994]. The general rainfall process over the mountainous areas is associated with orographic lifting as low-level flow passes over the terrain. One mechanism consists of rising air that cools adiabatically, releasing moisture as precipitation on the windward side of mountain. On the other side of the mountain, the air descends and warms, drying as precipitation dissipates. As a consequence, precipitation in mountainous areas has increased in some region and decreased in others. An important characteristic of precipitation in mountainous areas is its relationship to elevation. Total precipitation generally increases with elevation up to a certain height, and then begins to decrease above that elevation on a mountain's upwind sides. Information on the variation of precipitation with elevation helps in providing a realistic assessment of water resources, estimation of maximum precipitation, and hydrological modeling of mountainous regions [*Barros et al*., 2006]. In recent years, spatial variability in precipitation has received attention for studying the interactions among climate, erosion, and tectonics [e.g., *Anders et al*., 2006; *Barros et al*., 2006; *Bookhagen*, 2010]. Furthermore, it is hypothesized that an increase in rainfall variability in the major mountainous region is an important indicator of global climate change, because mountain environments are particularly vulnerable to such changes.

Direct measurements of precipitation in mountain environments are particularly challenging, because of the need to cover a large range of elevations and orographic positions. In addition, in the mountainous regions, it is often difficult to install rain gauges at upper elevations because hillslopes are steep, weather is harsh, and lack of roads and transportation make the collection of precipitation data difficult. On the other hand, the physiographic features and the complex atmospheric processes significantly modify the distribution of precipitation. Hence, in the mountainous areas where large variability in the precipitation exists, the gauge network is never adequate to define the detailed precipitation distribution (Daly 1991).

Several studies have been conducted on the distribution of rainfall with elevation in various regions of the world [e.g., *Barros and Lattenmaier*, 1993; *Bookhagen and Burbank*, 2006; *Bookhagen and Strecker*, 2008; *Dairaku et al*., 2003; *Dhar and Rakhecha*, 1981; *Linsley et al*., 1949; *Rumley*, 1965; *Sokol and Bližňák*, 2009; *Suprit and Shankar*, 2008; *Venkatesh and Mathew*, 2007]. These studies have shown that rainfall amounts generally increase with altitude up to a certain height on windward slopes. However, this relationship varies considerably with time and place. One prior study, using 50 rainfall stations, an attempt was made to ascertain the maximum elevation of increased rainfall in the central Himalayas during the monsoon season [*Dhar and Rakhecha*, 1981], showing that no linear relationship exists between rainfall and altitude and that the maximum rainfall zones fall near foothills at an elevation of 2.0–2.4 km.

Most of the previous studies on precipitation-elevation relationship were based on rain gauge data and were limited to basin scales [e.g., *Dhar and Rakhecha*, 1981; *Dairaku et al*., 2004, *Linsley et al*., 1949; *Rumley*, 1965; *Singh et al*., 1995, and *Singh and Kumar*, 1997; *Suprit and Shankar*, 2008]. However, gauge networks are considered insufficient for vast mountain topography and are subject to various types of inaccuracies, such as measurement and

representative errors. In this context, the Precipitation Radar (PR) onboard the Tropical Rainfall Measuring Mission (TRMM) revolutionized the global view of the distribution and mechanisms of precipitation by providing high spatial resolution with an ability to profile the vertical structure of precipitation. Despite a lack of high temporal resolution, this instrument revealed—for the first time—spatially robust patterns of precipitation distribution in the Himalayas [*Barros et al*., 2000; *Bookhagen and Burbank*, 2006; *Bookhagen and Burbank*, 2010; *Anders et al*., 2006; *Shrestha et al*., 2012], the Andes [*Bookhagen and Strecker*, 2008; *Nesbitt and Anders* 2009; *Buytaert et al*., 2006], and the South Asian coastal mountains [*Romatschke and Houze*, 2011a; *Xie et al*., 2006]. Though the several studies have already shown that rainfall amounts generally increases with altitude up to a certain height on windward sides, but it is still unclear about a key factor which determines the rainfall maxima over the higher elevation areas. Some studies [*Dairaku et al*., 2004a, 2004b, *Engman and Hershfield*, 1969; *Sokol and Bližňák*, 2009], utilizing observational data and numerical simulation found that larger quantities of rainfall recorded at higher altitudes could be attributed to greater duration and higher frequency of rainfall.

Aside from seasonal variability, intraseasonal fluctuations (often referred to as active/break cycles) of rainfall in the summer monsoon season is a substantial component of the South Asian monsoon rainfall, because uneven spatial and temporal variation of rainfall during JJA may have an adverse effect on agriculture. The existence of active and break periods is caused by latitudinal oscillations of a monsoon trough. During active periods, a monsoon trough region extends from the head of the Bay of Bengal heat low over Pakistan along the Gangetic Plains. In contrast, a monsoon depression occurs close to the Himalayan foothills during break periods, where the southeasterly flow from the Bay of Bengal, and the southwesterly flow from

the Arabian Sea branch meet and move northward [*Krishnamurthi and Shukla*, 2000; *Ramamurthy*, 1969]. The active monsoon rainfall is considered to be above normal over central India and below normal over the Himalayan foothills. This pattern is reversed during the break phase [*Krishnamurthy and Shukla*, 2000]. Several studies have described precipitation characteristics during active and break phases over central India and the Himalayan foothills [e.g., *Annamalai and Slingo*, 2001; *Singh and Nakamura*, 2010]. Subseasonal monsoon fluctuation is largely responsible for the spatial variation of rainfall over the southern slope of the Himalayas; however, no study has focused on each region to date. Information about variability in precipitation characteristics during active and break phases over the central Himalayan region (CHR) could improve understanding of Himalayan precipitation mechanisms.

1.2 Purposes and outlines of thesis

The main purpose of this study is to investigate the characteristics of summer precipitation around mountainous regions in south Asia and South America (Fig. 1). Primarily, our focus is on spatial distribution of precipitation climatology, with a particular focus on its relationship with elevations. In addition, temporal (seasonal and intraseasonal) variability of precipitation are also examined over the central Himalayan regions.

This thesis is structured as follows: Chapter 2 describes the description of data processed in this study and analysis methodology. Chapter 3 consists of spatiotemporal distribution of precipitation over the central Himalayan region. Chapter 4 presents characteristics of summer precipitation around the Western Ghats, Myanmar west coast and Andes. The results are summaries and discussed in Chapter 5. A general conclusion of this study is summarized in Chapter 6.

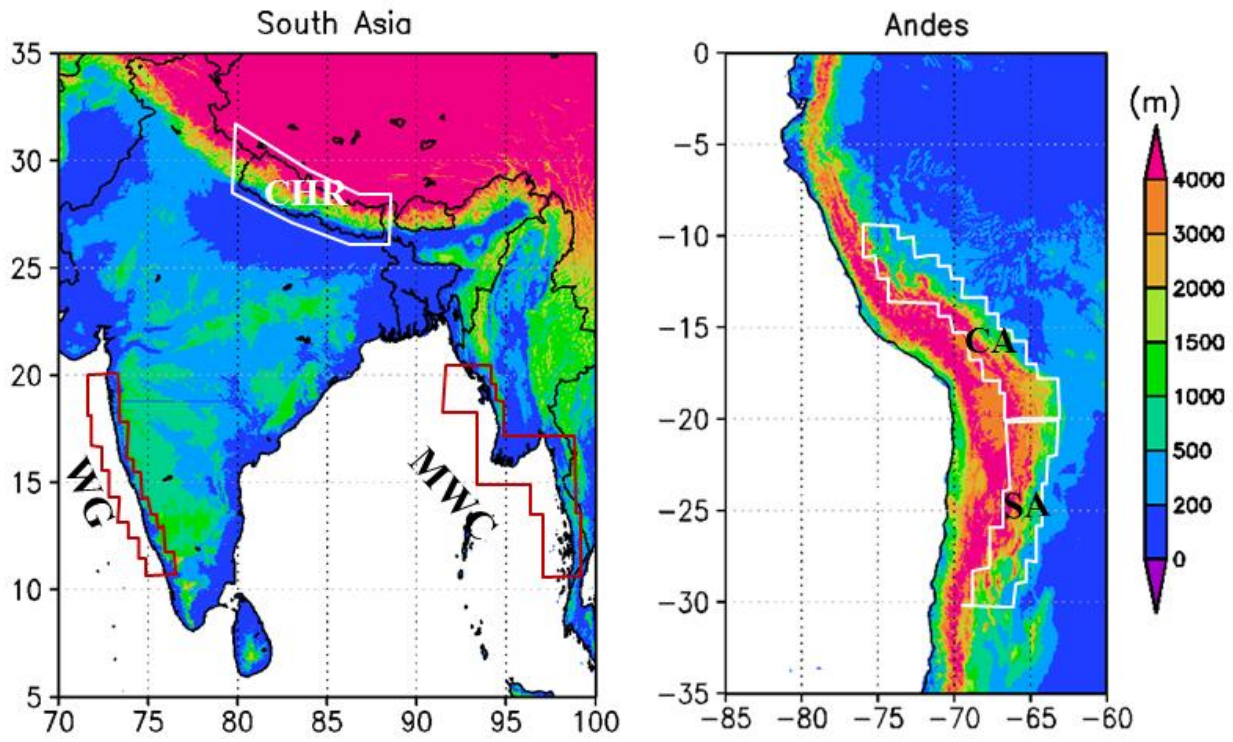

Figure 1. Topography of the region of interest: (a) South Asia, and (b) Andes. Subregions of study are: Central Himalayan region (CHR); Western Ghats (WG); Myanmar West Coast (MWC); Central Andes (CA); and Southern Andes (SA).

2. Data and Methods

2.1 Data utilized

2.1.1 TRMM

The Tropical Rainfall Measuring Mission (TRMM) is a joint mission between the United States National Aeronautics and Space Administration (NASA) and Japan Aerospace Exploration Agency (JAXA) launched in November 1997. The TRMM is specifically dedicated to monitoring rainfall in the tropics and subtropics (extending from 35°S to 35°N). The TRMM includes the first space-born precipitation radar (PR), a passive microwave imager (TMI), visible infrared scanner (VIRS), lightning imaging sensor (LIS), and a clouds and earth's radiant energy system. The first three instruments are designed to obtain rainfall and other relevant information (e.g., rain type, echo-top height, cloud type) individually.

In this study, the TRMM satellite's PR version 6 products have been processed for pre-monsoon (March–May; MAM) and summer monsoon (June–August; JJA) for 1998–2008 for use as primary data. Briefly, TRMM PR is the first spaceborne radar designed to provide three-dimensional maps of storm structures [*Kumerrow et al*., 1998, 2000]. PR has horizontal resolution of ~4 × 6 km and vertical resolution of 250 m at nadir with 215-km swath width operating at 13.8 GHz. It can detect reflectivities down to nearly 17 dBZ, equivalent to rain rates of ~0.5 mm/h. The pixel size, swath width, and sensitivity to rain changed slightly (5-km pixel size, 247-km swath width and sensitivity reduced by 1.2 dB) after an orbit boost from 350 km to 402.5 km in 2001. However, the differences are insignificant and are neglected in this study. To study rainfall patterns, product 2A25 [*Iguchi et al*., 2000] was used; it provides near-surface rain

rate from PR. “Near-surface” rain rate was obtained from the range bin closest to the surface that is generally not corrupted by surface clutter. The near-surface height ranged from 500 m above ground level (AGL) at nadir to 2000 m AGL at the edge of the observation swath. The average rain rate is calculated as a product of rain frequency (number of rain samples normalized by total number of samples) and conditional rain rate (near-surface rain rate only when it is raining). The storm height data were obtained from PR product 2A23. The TRMM 2A23 storm height product is based on the 18-dBZ (equivalent to approximately 0.5 mm h^{-1}) echo-top height. Storm height was calculated only when it was raining.

We used TRMM PR product 2A25 for rain-type classifications (copy of the 2A23 rain type field). The PR algorithm classifies the rain pixels into three categories: convective, stratiform, and others. This classification is based on the vertical pattern of the profile (known as the V-method; *Awaka et al*., 1997) and on the horizontal variability of the echo (known as the H-method; *Steiner et al.*, 1995). In brief, when a bright band is detected near the freezing level, the precipitation is classified as stratiform. If a bright band is not detected, and the maximum value of radar reflectivity in the beam exceeds 39 dBZ, rain type is classified as convective. When the precipitation type is neither stratiform nor convective, it is labeled as “other.” The “other” category represents either noise or regions of precipitation aloft with no precipitation near the surface.

Uncertainty

In generally, there are certain sources of error in the temporal average of TRMM PR-estimated rainfall, i.e., retrieval and sampling errors [*Anders et al., 2006*]. The former includes error in the remote-sensing methods, and the latter is related to the poor temporal resolution.

Sampling error depends primarily on sampling frequency. This is because a low earth orbit satellite is unable to provide continuous coverage of a given area. For a small number of samples, sampling error is likely to be more significant than retrieval error [*Bell and Kundu,* 2000]. Several researchers suggest that TRMM PR sampling errors are small (~10%) for monthly rainfall totals [*Anders et al*., 2006; *Bell and Kundu,* 2000]. A recent study by *Nesbitt and Ander*s [2009] notes that sampling error is small enough to resolve statistically significant precipitation patterns in regions with large precipitation totals. In this study, we compared results for the first half (1998–2004) and second half (2004–2008) of the study periods to check the consistency of our findings. Figure 2 illustrates the spatial variation of rainfall across the central Himalayas (84.5°E–85.0°E, 26.0°N–30.0°N) for MAM and JJA. During MAM and JJA in both halves of the study period, general patterns of rainfall are similar. This comparative analysis confirmed the consistency of basic findings.

2.1.2 Reanalysis Data

We used the Japanese 25-year Reanalysis (JRA-25) [*Onogi et al*., 2005] and Japan Meteorological Agency (JMA) Climate Data Assimilation System (JCDAS) datasets to examine synoptic conditions. The datasets are global in coverage, with 2.5° and 1.25° spatial resolution and 6-h temporal resolution. In this study, we primarily used monthly mean climatological normal values calculated from the JRA-25/JCDAS for 1981 to 2010 with a spatial resolution of 1.25^{o}.

2.1.3 Topographic Data

The Global 30 Arc-Second Elevation Data Set (GTOPO30) is regridded at 0.05° resolution from approximately 1-km global raster Digital Elevation Model (DEM) data

developed by the Earth Resources Observation Systems (EROS) Data Center of the United States Geological Survey (USGS). GTOPO30 was derived from several raster and vector sources of topographic.

2.2 Analysis Methods

Precipitation characteristics were investigated using rain rate, rain frequency, conditional rain rate, rain type, storm-top height, and vertical structure of rain rate. For data processing, we first binned data from each individual swath onto a regular grid with spacing of 0.1° (about a 1 × km, for the central Himalayan region) and 0.05° (about a 0.5 × 0.5 km, for the other subregions) . The gridded data were than averaged over the entire period of record to produce daily-mean climatologies.

For statistical analysis of altitudinal variations, precipitation characteristics were averaged for each 200-m altitude interval up to 5,000 m in the Himalayas and Andes. The analysis was restricted within 5,000-m elevation because some of the highest altitude pixels showed excessively high magnitudes of rainfall. For example, pixels that include the world's highest peaks, Mt. Everest (8,848 m), Mt. Lhotse (8,516 m), and Mt. Cho Oyu (8,188 m), exhibited high rainfall totals of 4.95 mm/d. These high totals could be attributed to ground clutter contamination in radar echoes. Ground clutter occurs because of radar returns from higher terrain being misread as reflectivity owing to rain drops. Such contamination is more likely over steep slopes. This is because chances of reflection of the beam increase in areas of steep slope, as the incidence angle of the beam increases [*Anders et al*., 2006]. The effect of ground clutter contamination on the representation of spatial pattern of rainfall is small over lower elevation

mountainous regions [*Anders et al*., 2006; *Takahashi et al*., 2010]. Another reason to limit the area to altitudes below 5000 m elevation is simply to exclude the northern slopes of the Himalayas.

The area-averaged values were smoothed by a 1:2:1 smoothing filter. Smoothed values (SV) are given as

$$SV_a = \frac{V_{a-1} + 2V_a + V_{a+1}}{4},$$

where V and a represent the averaged value and altitude, respectively.

Identification of active and break periods

There have been several studies on active and break monsoon based on different criteria and locations [e.g., *Annamalai and Slingo*, 2001; *Gadgil and Joseph*, 2003; *Krishnan et al.*, 2000; *Rajeevan et al*., 2010; *Webster et al*., 1998]. Traditionally, active and break periods have been identified on the basis of surface pressure and wind patterns over the Indian region [e.g., *Dhar et al*., 1984; *Ramamurthi*, 1969; *Webster et al*., 1998; *Goswami and Ajayamohan*, 2001]. In several recent studies [e.g., *Annamalai and Slingo*, 2001; *Gadgil and Joseph*, 2003; *Rajeevan et al*., 2010; *Singh and Nakamura*, 2010], "breaks" (and active spells) are defined in terms of the rainfall over the monsoon zone during the mature monsoon months July–August. A different approach [*Krishnana et al*., 2000] used outgoing longwave radiation (OLR), which is a proxy for rainfall, to define breaks.

In this study, we used the TRMM 3B42 version 6 daily rainfall data for the 11-year period to identify active and break periods. TRMM 3B42 provides fine scale (0.25° × 0.25°, 3 hourly) data in a global belt extending from 50°S to 50°N latitude [*Huffman et al*., 2007]. This

product combines PR, multi-satellite passive microwave, and geostationary infrared rainfall estimates. The criteria defined by *Singh and Nakamura* [2010] were adopted to identify active- and break-monsoon periods but for different locations. This criteria defines active (break) phases when daily rainfall over the Himalayan foothills (82°E–86°E, 27°N–28.5°N and 86°E–90°E, 26°N–27°N) is more (less) than 0.5 standard deviations from the average of July–August for each year for a minimum of three consecutive days. The numbers of active and break days using our criteria were 83 and 144, respectively. In general, these active and break days were consistent with those identified by *Singh and Nakamura* [2010], although different locations were chosen for the study. Active and break spells existed in almost every monsoon; only one season (1999) did not have any active events. An average of 7.55 active and 13.09 break days was observed during July–August. Most of the active spells lasted 3–4 days, while more than 50% of the dry spells were of such duration.

3. Spatiotemporal variation of rainfall over the central Himalayan region

3.1 The central Himalayan region

Distinct topographic patterns exist in the Great Himalayas (Fig. 1a). The eastern and western Himalayas are characterized by one-step topography [Bookhagen and Burbank, 2006, 2010], i.e., the Himalayas without its subordinate Himalayas, with consistent increment in elevation. In contrast, the central region is characterized by two-step topography, i.e., topography that includes the major Himalayas and their subordinate Himalayas. Note that the major

Himalayas consist of the Lesser Himalayas and Greater Himalayas, and the subordinate Himalayas indicate the Sub-Himalayas (Fig. 2).

The study area (outlined by the thin black rectangle in Fig. 1) covers approximately 1,000 km and includes the most rugged portion of the complex Himalayan topography (approximately 2,400 km). The highly elevated central Tibetan Plateau is located to the north and the low-elevation Gangetic Plains to the south. The CHR is located approximately on the margin of 26.0°N–31.0°N, 80.0°E–88.5°E in South Asia. East of 84.0°E, the mountains run roughly in an E–W direction; to the west of 84.0°E, the mountain range is oriented in an ESE–WNW direction. The range is characterized by narrow and sharply uplifted topography from south to north with a remarkable arrangement of parallel mountain chains. Elevation varies from approximately 60 m above mean sea level (AMSL) in the southern (Terai) plane to 8,848 m (Mt. Everest) in the northeast within a few tens of kilometers. Such extreme variation in altitude leads to a wide range of climatic conditions. Within the Himalayas, climate varies depending on elevation and location: the climate ranges from tropical at the base of the mountains to cold alpine at the highest elevations.

Physically, the CHR forms three sub-parallel zones: the Greater Himalayas (GH), the Lesser Himalayas (LH; also known as the Mahabharat Range), and the Sub-Himalayas (SH; known as the Siwalik Range). The parallel ranges may exert a significant influence on monsoon and rainfall pattern [e.g., *Anders et al*., 2006; *Bookhagen and Burbank*, 2006, 2010]. The SH (~500–1,200 m AMSL) is the southernmost mountains in the Himalayan range, which is considered to be the first zone of heavy rainfall in JJA. The LH (1,200–3,000 m AMSL) is located between the SH and GH, where rainfall activity is more concentrated. Small valleys are oriented in the E–W direction between the SH and LH. The GH (over 3,000 m AMSL) is located

north of the LH, and is characterized by less rainfall activity; however, the region experiences significant snowfall during winter.

3.2 Spatial distribution of rainfall

First, we examined the spatial and temporal distribution of the rainfall around the Himalayas for MAM and JJA. Monthly average rainfall (expressed in mm/d) over 11 years (1998–2008) is shown in Figure 3, which indicates a clear contrast in horizontal distribution and magnitude of rainfall between MAM and JJA. It was observed that the greatest amount of rainfall occurred in JJA over the eastern Himalayan region and CHR. *Bookhagen* [2010], *Bookhagen and Burbank* [2010], and *Nayava* [1980] also noted that summer monsoon rainfall provides more than 80% of the annual moisture budget for the CHR. A clear double band of rainfall maxima exists in JJA, but is absent in MAM over the CHR (Fig. 3a). Interestingly, high rainfall was observed in the higher terrain over the CHR in MAM. During JJA, a distinct feature of rainfall distribution was observed in the eastern, central, and western Himalayan regions (Fig. 3b). The eastern and western regions displayed a single zone of rainfall maxima; the eastern region showed high rainfall over lower elevation areas (below ~1,000 m AMSL); conversely, the western region exhibited high rainfall over higher elevation areas (above ~1,000 m AMSL). Previously, *Bookhagen and Burbank* [2006, 2010] found rainfall pattern in the eastern and western Himalayas to be characterized by singles peak over low-altitude areas. In contrast, the central region exhibited two zones of rainfall maxima. A comparatively narrow and continuous peak rainfall band appeared along the front of the low-elevation mountain range and a discontinuous and relatively broader band occurred along the steep slope of the LH. These

results are consistent with those of *Bookhagen and Burbank* [2006, 2010], who noticed double bands of rainfall maxima in the annual rainfall total.

Next, we examined storm height distribution over the Himalayas (Fig. 4). The actual storm height presented here corresponds to the height of the top of the precipitation column above ground level rather than AMSL. The correspondence between storm height and topography was clear in the eastern and western Himalayas, where tall storms were observed over low-altitude areas (Fig. 4a) in MAM. Over the CHR, storms were found to be shallow and disorganized. Compared with MAM, topography-dependent storms were noticed over the entire Himalayan region in JJA (Fig. 4b), which may indicate a less convective rain system in JJA. Results suggest that storms are shallow over higher elevation areas in JJA over both the eastern and central Himalayas, whereas a wide area of tall storms from lower to higher elevations were observed in the foothills of the western Himalayas. These tendencies are consistent with the occurrence of deep and wide intense convective processes in the western Himalayas and with wide convective and broad stratiform systems at the lower elevations of the central and eastern Himalayas [*Houze et al*., 2007]. An example of latitudinal variation of storm height during MAM and JJA in the central Himalayas is shown in Figure 4c. General patterns of storm height distribution are similar during both seasons. The storm height was about 6 km AMSL with a clear peak near the top of the slope and a small peak at the bottom. Note that there is less latitudinal variability of storm height with a relatively smaller standard deviation in the summer monsoon season compared with the pre-monsoon season.

A considerable amount of spatial and temporal variability in the rainfall distribution around the Himalayas was noted. Some studies [e.g., *Bookhagen and Burbank*, 2006, 2010] explained that spatial variability in JJA is greatly attributed to the distinct topography of the

Himalayas. The CHR comprises a frontal low-altitude mountainous range and inner major mountain topography. As evident in our results, the double bands of rainfall maxima correspond to these two significant rises in topography, particularly in JJA. Thus, the spatiotemporal variations of rainfall and their mechanisms are likely to differ from other regions of the Himalayas.

We now focus on unique features of the spatiotemporal variation of rainfall in the CHR. Essentially, the lower and higher elevation areas mentioned in this chapter refer to the zones of the primary rainfall peak along the SH and the secondary rainfall peak in the LH, respectively.

3.3 Rainfall frequency and conditional rain rate

Most of the previous studies have investigated only climatological mean rainfall patterns. However, it is unclear whether the amount of rainfall is caused by a larger number of weaker rainfall events or a smaller number of stronger rainfall events. The differences should be a reflection of the precipitation mechanism, which is an interesting subject for research. In addition, such differences are relevant to society; for example, strong but rare precipitation tends to cause more damage. Therefore, we discuss the rainfall frequency, conditional rain rate, and vertical structure of rainfall in this subsection.

In MAM, the conditional rain rate was approximately 3–5 mm/h (Fig. 5a), which is slightly higher than or equal to that in JJA (Fig. 5c); however, the frequency was remarkably lower in MAM (Figs. 5b and 5d). Hence, less frequent rainfall activity can be considered a cause of the rainfall minima in MAM. Over the LH, rain frequency was approximately 6%–12%,

which is two times as frequent as that rain over the low-elevation areas. Although a high conditional rain rate appeared over low-altitude areas, a smaller amount of rainfall was observed, suggesting that the higher elevation area received a larger amount of rainfall caused by a higher frequency of rainfall. In JJA, the conditional rain rate was greater than 3 mm/h and the frequency of rainfall was approximately 9%–12% in lower elevation areas, while the conditional rain rate was less than 3 mm/h and the frequency of rainfall was approximately 12%–18% over higher elevation areas. These findings indicate that the rainfall maxima over higher elevation areas are the result of a higher frequency of rainfall and that those over lower elevation areas are the result of both high conditional rain rate and high rain frequency. These findings agree well with the results of *Dairaku et al*. [2003] based on the data obtained from 15 rainfall stations in the Mae Chaem watershed, Thailand.

To more precisely quantify the relationship between rainfall characteristics and altitude, we analyzed area-averaged total rainfall, rain frequency, and conditional rain rate over the southern slopes of the Himalayas up to 5,000 m elevation. Averaged values of all three components for each 200-m elevation area are presented in Figure 6. No clear rainfall peak was evident in MAM, although a slightly higher broad peak was observed over higher altitude areas (Fig. 6a). This feature is different than that typically observed in JJA periods. The two rainfall peaks, previously observed by *Bookhagen and Burbank* [2006], have been observed in JJA. The primary peak of total rainfall appeared at a mean elevation of 500 m (AMSL) and the secondary peak appear at a mean elevation of 2,100 m (AMSL) (Fig. 6b). The figure shows that the conditional rain rate decreases as altitude increases, whereas the frequency of rainfall increases as elevation increases, up to a certain altitude. These results demonstrate that the high-altitude rainfall peak is followed by more frequent rainfall rather than a high conditional rain rate.

Despite fewer rainfall events, a low-altitude primary rainfall peak was noticed, which indicates that strong rainfall events contribute to a larger amount of rainfall over lower elevation areas.

Figure 7 depicts the vertical cross section of rain rate during MAM and JJA. That storm top reached above 12 km in height suggests a deep convective system, particularly over the SH and the southern plains in MAM (Fig. 7a). The tall storm height in the CHR is consistent with *Romatschke and Houze's* [2011b] finding of more convective-type rainfall during pre-monsoon in the central Himalayan foothills. In JJA, rain-top height is lower and more homogeneous (Fig. 7b). Such patterns in storm height suggest that there is pronounced persistent rainfall and this could cause higher total rainfall. Compared with the low-altitude regions, the high-altitude regions experience lower rain-top height.

3.4 Rain-type distribution

Mountains can generate both stratiform precipitation, which occurs in a statically stable atmosphere, and convective precipitation, which results from the release of static instability. Thus, considerable spatiotemporal variation in rain type is also expected over the CHR. Information about rain-type distribution could provide valuable insight into rain systems. Pre-monsoon rain systems are most convective, whereas summer monsoon systems are more stratiform in the CHR [*Romatschke and Houze*, 2011b]. Figure 8a shows the difference in the conditional rain rate between stratiform and convective rain in JJA. Relatively larger and smaller differences were detected in the low- and high-terrain areas, respectively, which suggests a strong convective rain over the frontal low-altitude topography. Similarly, the difference in the occurrence of stratiform and convective rain events (number of stratiform/convective rain pixels)

is shown in Figure 8b. A large difference appeared over the higher elevation area, indicating that the maximum number of stratiform rainfall events occur over higher terrain. Furthermore, an area-averaged analysis of rain-type characteristics in JJA showed a linear increase in the occurrence of stratiform rainfall as altitude increases up to 2,200 m elevation (Fig. 9a), inferring that an area of high-rainfall frequency coincided with an area of active stratiform rainfall. This tendency is consistent with the higher percentage of convective rain over lower terrain, and more stratiform rain over higher terrain [*Romatschke and Houze*, 2011a]. In conclusion, higher topography favors frequent but less intense stratiform rainfall, which leads to rainfall maxima in the LH, whereas lower terrain receives high rainfall amounts as a result of strong convective rainfall (Fig. 9b).

3.5 Active- and break-period rainfall distributions

MAM is characterized by a dry atmosphere compared to that of JJA. The seasonal variation described in the previous section may be similar to the variation in active and break periods in the mature monsoon season. Thus, we examined the variation of rainfall characteristics during active and break periods.

The composite map of wet and dry phases for 11 consecutive summers over the Himalayas is similar to that of *Singh and Nakamura* [2010] (figure not shown). During active periods, rainfall increased around the southern slopes of the Himalayas and decreased over Indian plains, particularly over central India. In contrast, the opposite scenario occurred during dry periods. More interestingly, distinct features were observed even within the southern faces of the CHR and their surroundings during active and break phases. A high amount of rainfall was

recorded only during active periods over the Himalayan foothills; however, higher elevation areas apparently experienced high rainfall even in dry periods. The high rainfall during active periods tends to be more persistent with lower echo-top height in the SH than in the LH (Fig. 10a). Overall, the rainfall during the active period has higher echo-top than that during the break period (Fig. 10b). The lowering of the echo-top height in the break periods may be because of the greater number of shallow convective storms [*Singh and Nakamura*, 2010].

Details of statistical outputs of altitudinal patterns of rainfall characteristics are presented in Figure 11. During active periods, the daily rainfall reached 24 mm/day over the SH, which is significantly higher than the mean monsoon daily rainfall (~13 mm/day), whereas much less rain (~5 mm/day) was observed during the break period (Fig. 11a). On the contrary, no significant difference was detected in rain totals over the LH. A prominent feature in total rain distribution is the linear decrease (increase) during the active (break) period up to a certain altitude, which implies that the rainfall amount over the SH was mostly dependent on active-period rainfall; however, both periods affected the LH. Further, these results confirm that there are fewer rainy days in low-altitude regions than in higher altitude regions. The percentage of active- and break-periods rain was investigated to observe the contribution of active and break period rainfall to overall mature monsoon rainfall (Fig. 11b). The "percentage of rain" was defined as the percentage of total rainfall amount in active/break period to summer monsoon rainfall total. Our observations suggest that the active-phase rainfall was dominant (>20%) in JJA rainfall total over the SH. However, on an average, there were fewer active days (7.55 days) than break days (13.09 days). In contrast, break-period rainfall was dominant above 1,700 m elevation. Figure 11c shows the altitudinal variation of the rain-conditioned rain rate for active and break periods. The patterns for both were similar; that is, heavy rainfall occurred over low-

altitude regions and decreased with increasing altitude. Figure 11d shows the altitudinal variation of rain frequency for active and break periods. During active periods, a peak appears over the southern slope of the SH; during break periods, a broad peak is observed over the LH. These patterns are exactly to the same as those of the rain rate. Thus, it is suggested that rain frequency is mainly responsible for altitudinal variation of rainfall over the Himalayas during both periods. In summary, the general pattern of active- and break-phases rainfall characteristics was similar to that observed in the summer monsoon and pre-monsoon seasons.

3.6 Atmospheric conditions

Here, we discuss the climatological context of atmospheric system during MAM and JJA. The horizontal and vertical structure of the pre-monsoon and summer monsoon circulation was examined to understand precipitation mechanisms. The Himalayan range is located nearly in the meridional wall and provides a huge barrier to flow, tending to block the flow and cause convergence. The summer monsoon circulation pattern is markedly different from that of the pre-monsoon over the Himalayas. There is a strong, moist, low-level southeasterly wind from the Bay of Bengal region in the summer monsoon season (Figs. 12a). Moreover, the lower tropospheric climatology of wind at 925 hPa from JRA-25 reanalysis showed clear cyclonic circulation in the vicinity of the Himalayas. In contrast, northwesterly flow is apparent near the Himalayan foothills during pre-monsoon (figure not shown). Examination of equivalent potential temperature (commonly referred to as theta-e, i.e., θ_e) reveals higher value (~360 K) near the foothills of the Himalayas. This fact suggests that there is humid atmospheric conditions in these regions. Convective activity due to orographic lifting is an important factor in the generation of

rainfall over mountains [*Chater and Sturman*, 1998]. The difference in equivalent potential temperature between two pressure levels (925 and 600 hPa) over the area of interest (Figs. 12 and 13) was used to understand the strength of atmospheric instability (AI). The climatology of the atmospheric vertical structure from the JRA-25 reanalysis suggested weak AI in MAM (figure not shown). During JJA, the AI was relatively strong (above 14 K) (Fig. 12b) compared with MAM (~10–12 K). This is consistent with the findings of *Bhatt and Nakamura* [2006]. We did not observe a strong AI in the long-term climatological data during MAM, although intense rainfall was noted (Figs. 5c and 7a). This is probably because of the lower number of precipitation systems. Most days were without precipitation, and only a few systems with intense rainfall developed during the late pre-monsoon seasons. Thus, we checked the vertical structure for selected rainfall events during May in 2004 (days: 16, 17, 20, 21, and 28). Daily rain totals during those days were more than 0.5σ from the average of MAM. Figure 12c shows the composite of horizontal structure of atmospheric conditions at 925 hPa (equivalent potential temperature, relative humidity, and wind vector) during those days. There appears to be a strong instability (~26 K) with higher theta-e in the lower atmosphere over the southern plains and foothills of the Himalayas (Figs. 12c and 12d). Although the theta-e is higher over the southern plains, the specific humidity is lower (~14 gm/kg). This indicates that the high theta-e can be attributed to the high temperature of rather dry air. Similar characteristics were also noticed during major rainfall events in previous and successive years (figures not shown).

Figure 13 shows the composite of atmospheric conditions during active and break periods for 11 years; their distributions are remarkably similar, except for the horizontal wind component. During active phases, southwesterly flow from Arabian Sea and southeasterly flow from Bay of Bengal confluences near the eastern foothills of the central Himalayas (13a), but

apparent easterly flow (in other words steady flow parallel to mountain ranges) in break periods (Fig. 13b). These tendencies are in good agreement with low-level convergence (divergence) during active (break) periods along the Himalayan foothills (figure not shown). The difference in equivalent potential temperature (θ_{e925} - $\theta_{e600)}$ in active periods was slightly lower (~10–14 K) than that in break phases (~14–20 K), indicating higher atmospheric stability during the active monsoon. However, there is slightly more moisture in the lower atmosphere during active periods. The abundant supply of the moisture due to southeasterly flow in the active periods provides favorable conditions for generation of precipitation systems near the SH.

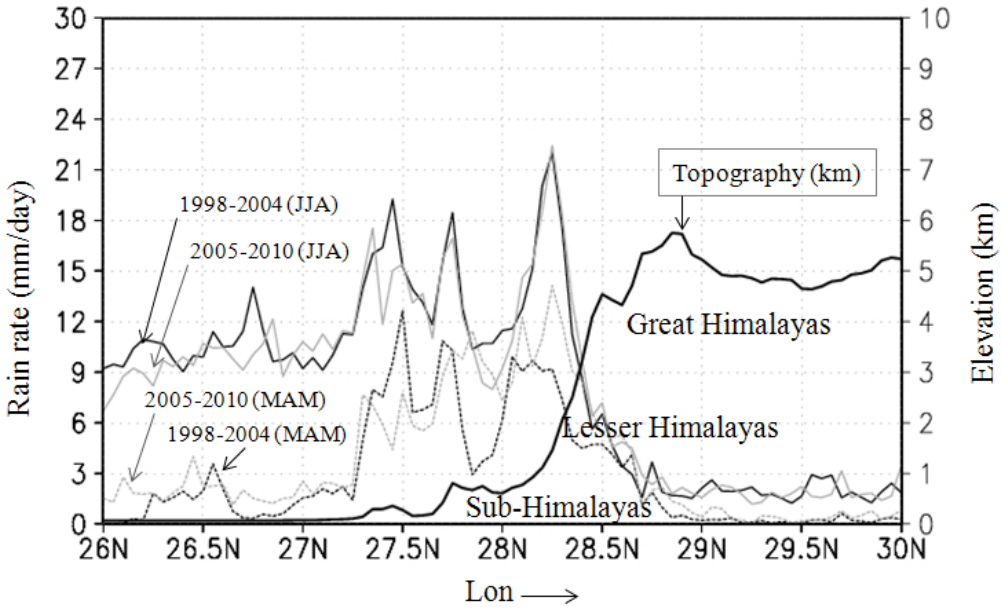

Figure 2. Rain rate distribution across the central Himalayas (84.5°E–85.0°E, 26.0°N–30.0°N) during pre-monsoon (MAM, dotted lines) and summer monsoon (JJA, solid lines) season for the first half (1998–2004, black lines) and second half (2005–2010, gray lines). Bold, heavy line represents topography for the same location.

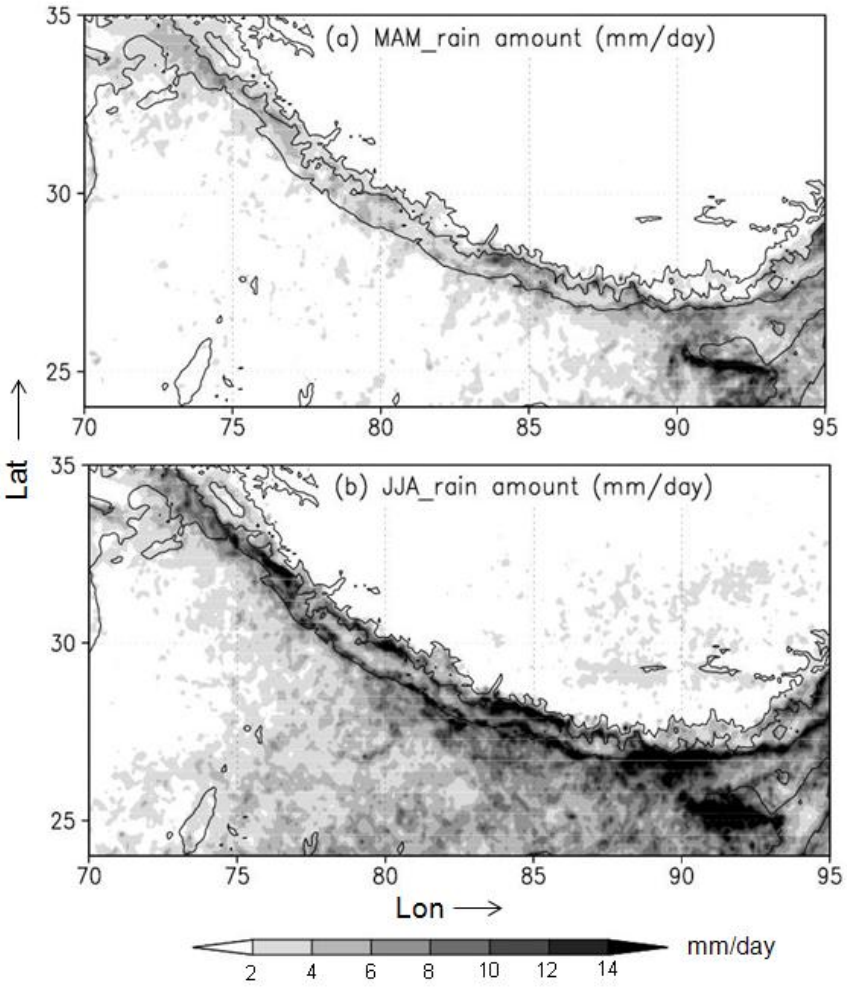

Figure 3. Distribution of rainfall amount in the 11-year period (1998–2008) in mm/day for (a) pre-monsoon (MAM); and (b) summer monsoon (JJA). Contour lines indicate 500, 2000, and 4000 m elevations.

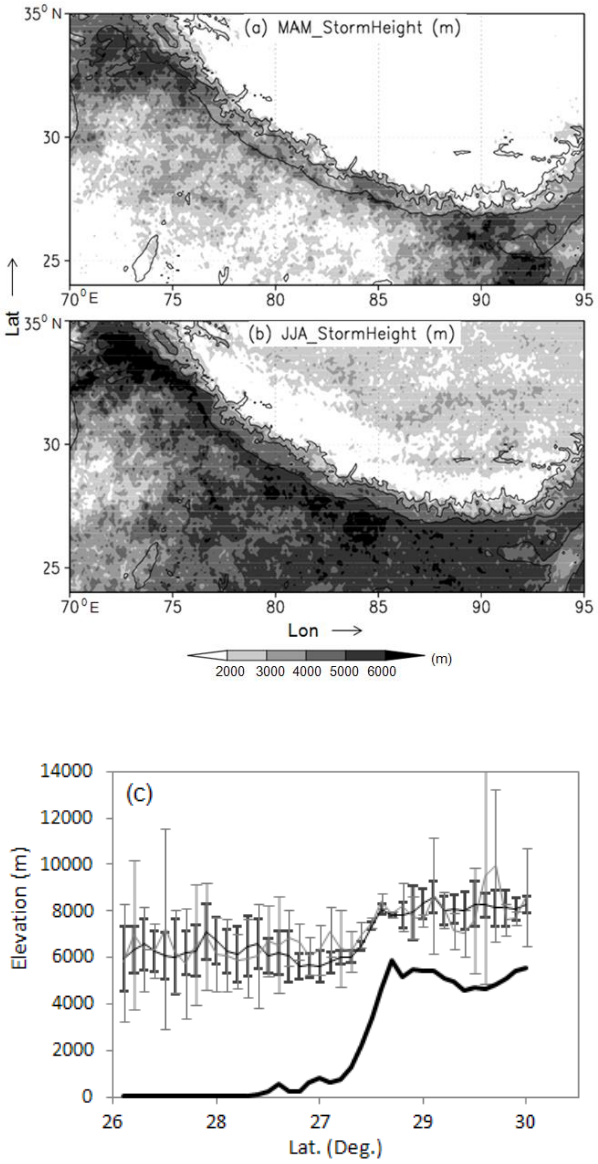

Figure 4. Horizontal distribution of actual storm height for (a) pre-monsoon (MAM) and (b) summer monsoon (JJA). Storm height (m) is calculated above the ground level instead of the sea level. (c) Mean storm height (above mean sea level) distribution across the central Himalayas (84.5°E–85.0°E, 26.0°N–30.0°N) with standard deviation plotted (shown by error bar) during MAM (gray line) and JJA (black line). Bold solid line represents topography for the same location. Contour lines represent 500, 2000, and 4000 m elevations.

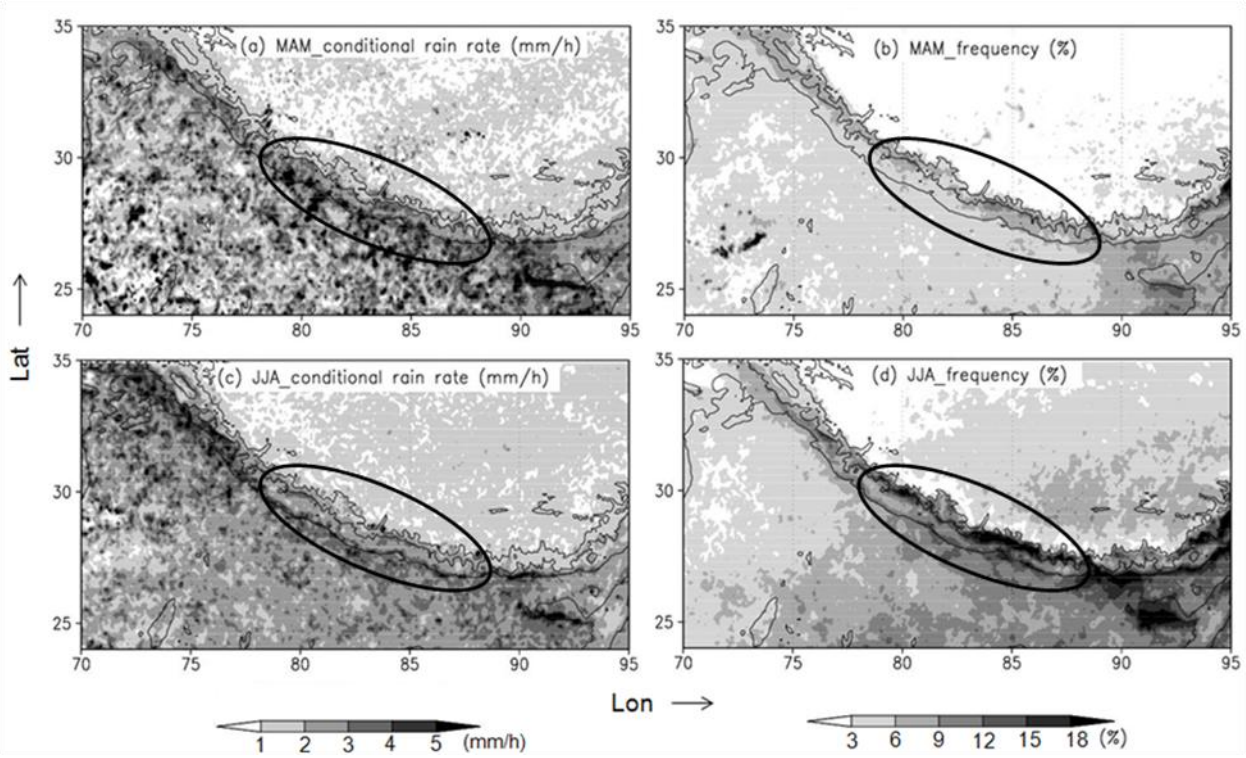

Figure 5. Horizontal distribution of rainfall characteristics for pre-monsoon (MAM) and summer monsoon (JJA). (a) Conditional rain rate for MAM (mm/h), (b) frequency of rainfall for MAM (%), (c) conditional rain rate for JJA (mm/h), and (d) rain frequency (%) for JJA. The area enclosed by the black oval lines represents the central Himalayan region (CHR).

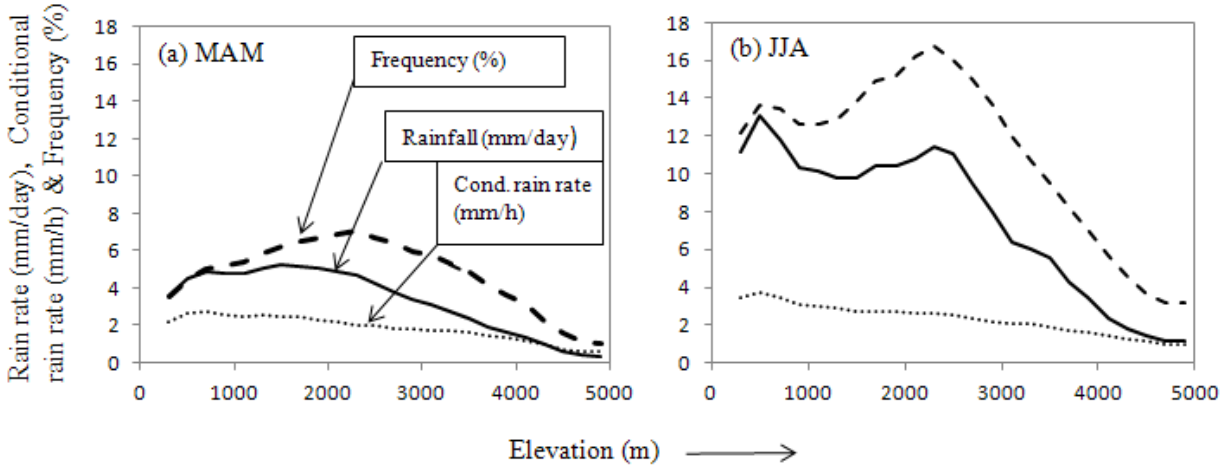

Figure 6. Variation of rainfall characteristics (rainfall, conditional rain rate, and rain frequency) with elevation for (a) pre-monsoon (MAM) and (b) summer monsoon (JJA). Solid, dotted, and dashed lines represents daily rainfall total (mm/day), conditional rain rate (mm/h) and frequency of rainfall (%), respectively.

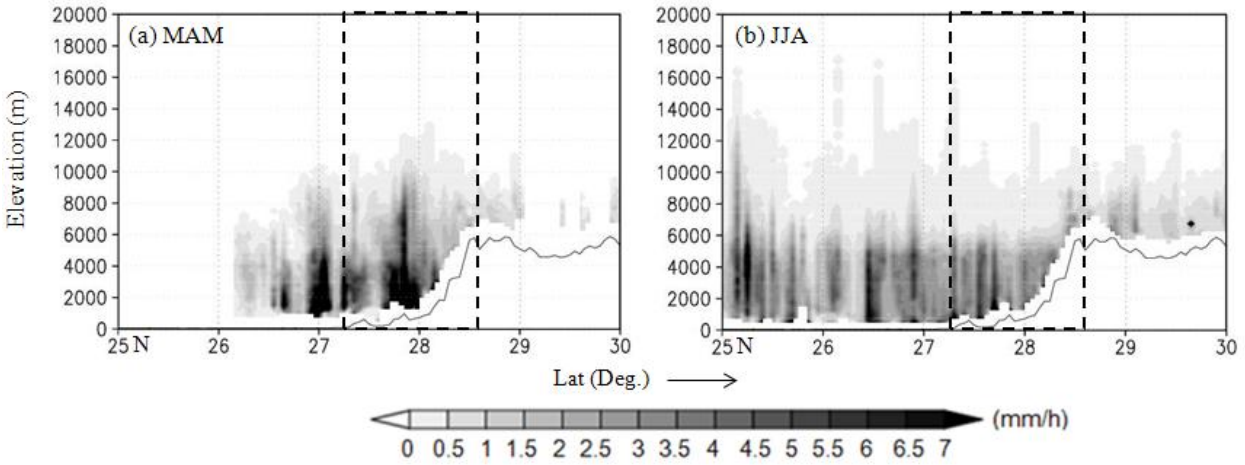

Figure 7. Vertical structure of rainfall (mm/h) at 84.5°E for (a) pre-monsoon (MAM) and (b) summer monsoon (JJA). Dashed rectangle indicates cross section of study area over the southern slopes of the Himalayas. Gray line represents north-south Himalayan topography at the same location.

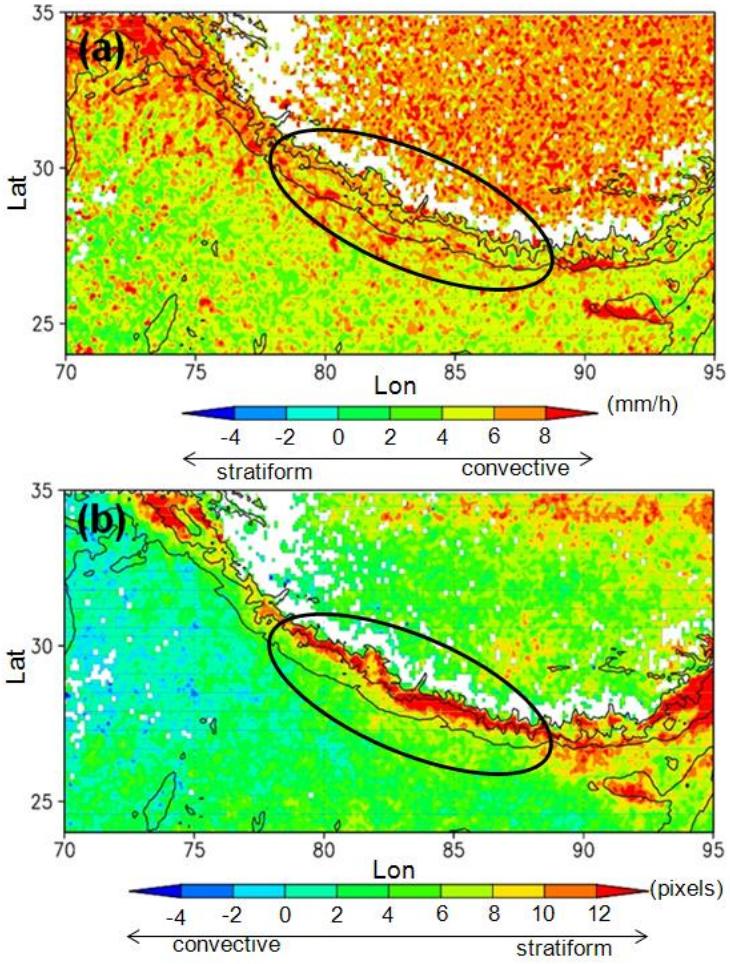

Figure 8. Horizontal distribution of rainfall types during summer monsoon (JJA). (a) Difference between the convective and stratiform rain rates (mm/h), (b) difference between the occurrence of stratiform and convective rain events. The area enclosed by the black oval lines represents the central Himalayan region (CHR).

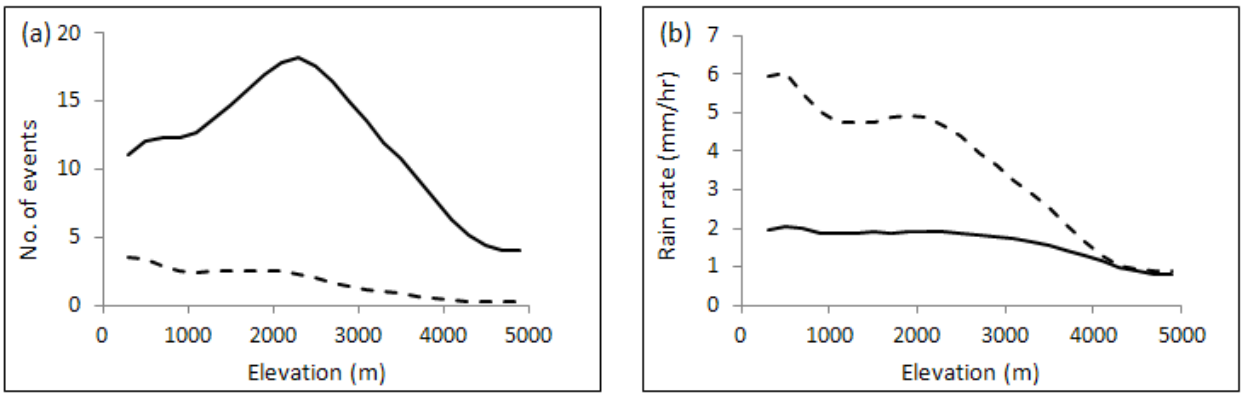

Figure 9. Altitudinal variation in rain type during summer monsoon (JJA) for (a) occurrence of rain events (pixel) and (b) rain rate (mm/h). Solid and dashed lines indicate stratiform rainfall and convective rainfall, respectively.

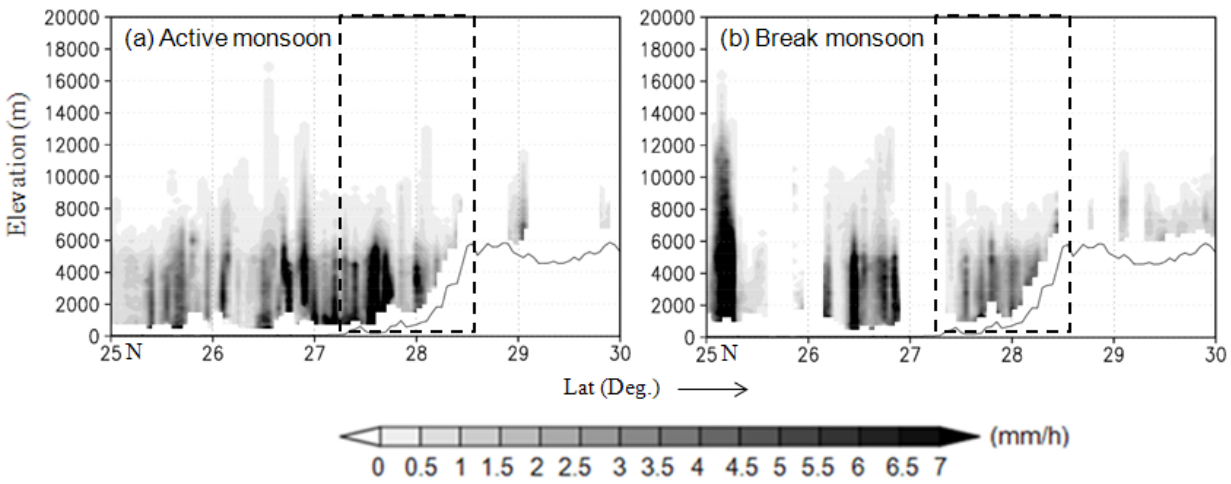

Figure 10. As in Fig. 7, but for (a) active monsoon and (b) break monsoon.

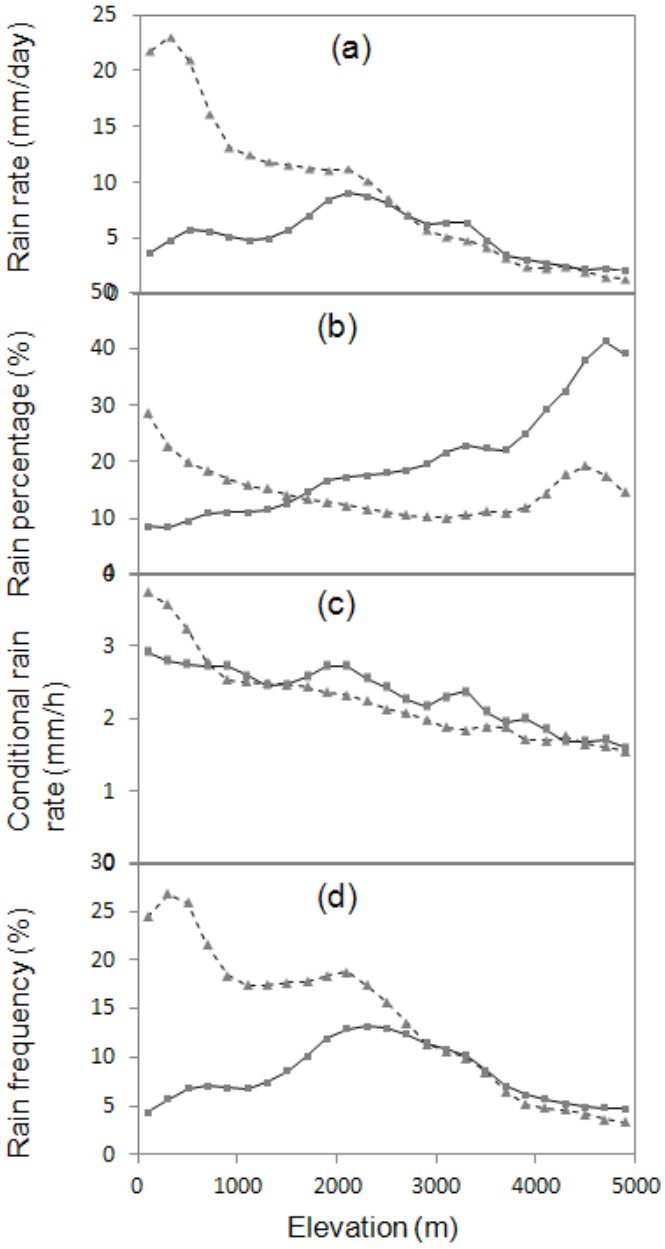

Figure 11. Altitudinal variation in rain characteristics during active (dashed line) and break (solid line) periods for (a) rain total (mm/day), (b) active/break rain percentage (%), (c) rain-conditioned rain rate (mm/h), and (d) frequency of rain (%).

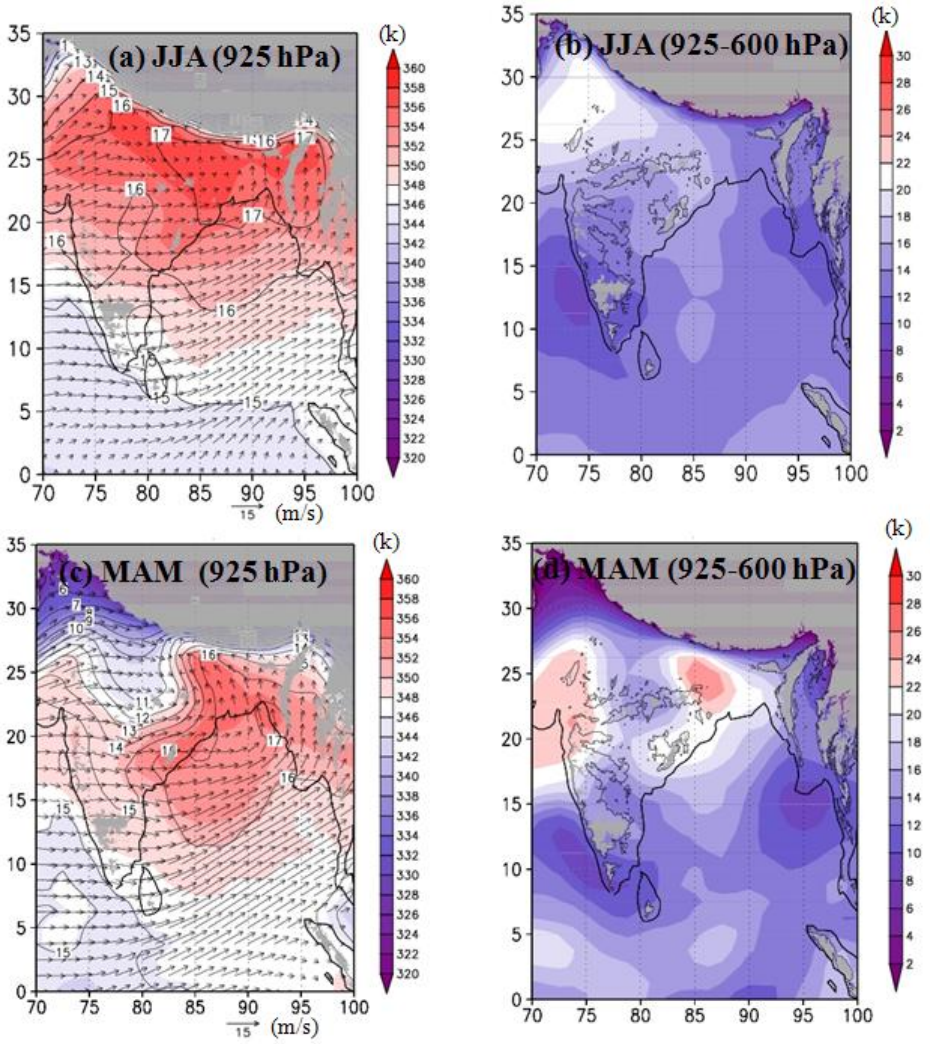

Figure 12. Horizontal patterns of equivalent potential temperature (K; color shaded), winds (m/s; black arrows), and specific humidity (g/kg, black contours) at 925 hPa for (a) JJA climatological mean and (c) MAM case study. Difference in equivalent potential temperature between two pressure levels (925 and 600 hPa) for (b) JJA climatological mean and (d) MAM case study. Gray shading represents topography above 800 m (~925 hPa).

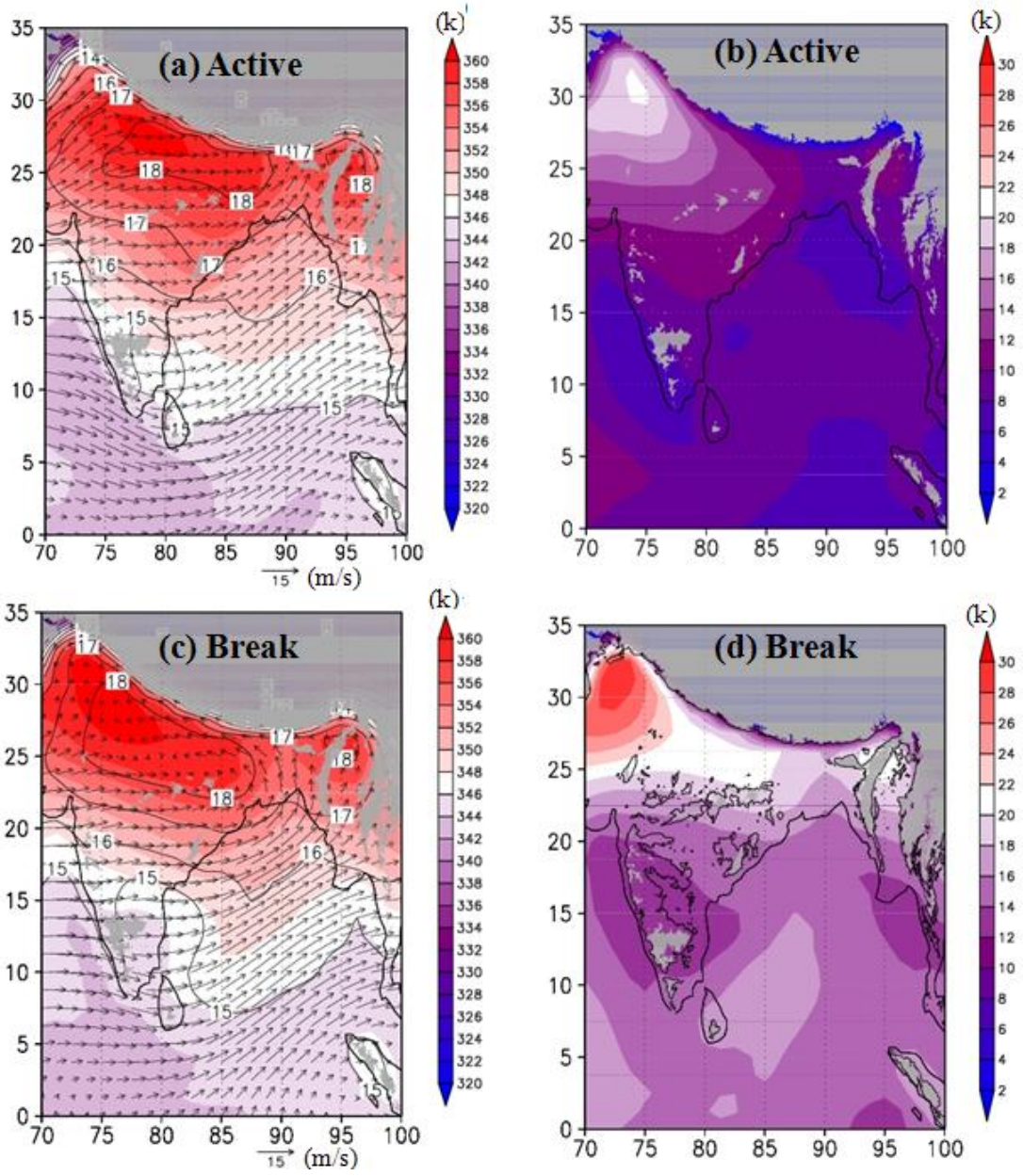

Figure 13. As in Fig. 12, but for (a) and (b) active monsoon, and (c) and (d) break monsoon.

4. Characteristics of summer precipitation around the Western Ghats, Myanmar West Coast, Andes

Figure 1 illustrates the region of interest, geographical features, and specific areas of study. We will discuss Andean precipitation separately since it occurs over land, and the western coasts of India and Myanmar will be discussed together because of their common features.

4.1 Coastal regions

4.1.1 Horizontal patterns of rainfall

The west coasts of India and Myanmar are the areas receiving the heaviest precipitation of the south Asian summer monsoon (*Hoyos and Webster* 2007; *Xie et al*. 2006). In both the WG and MWC regions, the maximum rainfall zone forms along a tight line on the windward side of the coastal mountains (Figs. 14a and 14b), as previously reported [*Biasutti et al*., 2011; *Romatschke* and *Houze*, 2011a]. Rainfall primarily occurs along the windward side of the coastal mountains, and propagates in an offshore direction. This finding is in contrast to the previous investigation using coarse-resolution datasets, which indicated an offshore maximum precipitation in the WG region [*Grossman and Durran* 1984]. In addition, by utilizing TRMM PR data at 0.5° resolution, *Xie et al*. (2006) noted that the location of maximum rainfall was displaced from the mountain slopes by approximately 50 km. At this fine resolution, it is apparent that the rainfall maximum is not displaced from the mountain slopes [*Biasutti et al*., 2011]. Although similar features of rainfall patterns are observed over both regions, the MWC region shows a wide area of maximum rainfall. A typical feature is observed in the WG region,

where maximum rainfall occurs around 500 m above mean sea level (AMSL) along the entire mountain range. Interestingly, the amount of rainfall over the Deccan Plateau to the east of WG, the down-wind side of the west coast of Myanmar Mountain and Irrawaddy river basin, is insignificant. However, the mountains in the both WG and MWC are not very high. This is accounted for by the classic rain-shadow effect of the corresponding mountain ranges.

The patterns of rain frequency were generally similar to the distribution of rain rate in both regions, with a larger and more homogeneous width of the coastal maxima (Fig. 14b). The most frequent precipitation, by far, was seen over the MWC regions. Although the western coast of Myanmar is a region of steep orography, the large spatial extent of higher rain frequency suggests effects other than orographic enhancement [*Bisautti et al*., 2011]. Numerical simulation by *Xie et al*. [2006] pointed that mesoscale heating interacts with large-scale circulation to force a broader rainfall maxima over the Bay of Bengal. In contrast, intense rainfall (>4 mm/h) was primarily observed offshore (Fig. 14c). The conditional rain rate was higher over the MWC compared with WG. This is consistent with the distribution of mean conditional reflectivity at the surface shown by *Bisautti et al*., [2011].

Figure 14d illustrates the horizontal distribution of storm top height over the study area during JJA. The actual storm height presented here corresponds to the height of the top of the precipitation column above ground level rather than MSL. Interestingly, a higher storm top appears over the broader area of the open ocean and western coast of Myanmar in the eastern Bay of Bengal. This is consistent with the greater probability of a wide convective core and broad stratiform region in the Bay of Bengal shown by *Romatschke et al*. [2010]. Note that the taller storms were observed only over the coastal ocean in both coastal regions, suggesting that intense rainfall offshore is due to deeper precipitation systems. Over the coastal mountainous

region storms are generally shallower than those over the adjacent ocean. This tendency is similar to that of taller storms over the Gangatic plains and shallower storms over the higher Himalayas [*Shrestha et al*., 2012). Although the conditional rain rate is higher in the coastal mountains, storm-top height is significantly lower. This is probably related to weak convection.

Evaluating rainfall characteristics along swath profiles is advantageous for investigating precipitation distribution in response to topography. Seven swath profiles, three from WG and four from MWC, roughly perpendicular to the respective coastal mountains were selected. Each swath profile is approximately 50-km wide × 500-km long. Rain characteristics and elevation along one profile represent the average over the width of the profile. All seven profiles illustrate the orographic effect of the coastal mountains, although there are noticeable differences in peak locations between WG and MWC (Figs. 15a and 15b). Over the WG regions, two distinct rainfall peaks appear in all swath profiles. The first peak is located a few km off the western coast of India, while the second major peak appears near the top of the mountain ranges. Offshore peaks are generally associated with conditional rain rate, while mountain rain peaks primarily corresponds to rain frequency. This feature is consistent with the precipitation distribution in the central Himalayas, where an intensity-dominated, low-altitude rainfall peak and a frequency-dominated, higher-altitude peak were identified by *Shrestha et al*. [2012]. Similarly, the MWC region also illustrates the maximum rainfall occurring near the top of the mountains, but the rain frequency does not correlate well to the maximum rainfall zone. In contrast, a broad peak of rain frequency extended from the mountain front to hundreds of km off the coastline over the MWC regions.

Analysis of storm-type distribution is more important over inhomogeneous regions, because it is directly related to precipitation mechanisms. The spatial patterns of stratiform and

convective rain are generally similar in both regions (Figure not shown). Figure 16 shows the difference in daily rainfall amount between convective and stratiform rain. A clear, large difference was detected over the slope of WG, typically along the 500-m contour line, which suggests that a large fraction of rain comes from convective systems. This feature is consistent with the findings of *Romatschke and Houze* [2011a], who showed that the WG is an exceptional area where precipitation systems are mostly convective. Over the MWC, stratiform and convective precipitation makes almost equal contributions to total rainfall. The tendency of precipitation maxima to occur where a large stratiform region was formed in association with extreme convection has been noted previously [*Romatschke and Houze* 2010]. For detail understanding of storm-type distribution, frequency and conditional rain rate are investigated for both stratiform and convective rain (Fig. 17). Stratiform rain is most frequent in the MWC region (Fig. 17a), whereas convective rain is most frequent the WG (Fig. 17b). Although the higher frequency of convective rain appears along a certain height of the WG, there is intense convective rain along the coastline of the western coastal region of India (Figure not shown). This difference in location of maximum rain frequency and conditional rain rate of convective rain suggests that maximum precipitation over WG is primarily attributed to frequent, but relatively weak, convection. In contrast, much more intense convective rain (>8 mm/h) is observed over broader area of MWC region, including coastal mountain and open ocean (Figure not shown).

4.1.2 Vertical profile of rain rate

The TRMM PR provided a vertical profile of rainfall, which is very important in studying the vertical structure of rain corresponding to a particular rain rate. This profile represents rainfall accumulated from each layer. Here we discuss the vertical profile of rain rate

from 2 to 16 km during JJA for all, stratiform, and convective rains, to understand the storm structure over the study area. The profiles are taken only for rain cases. We investigated the vertical profile of rain rate over the coastal ocean and coastal mountain separately, since echo-top height is higher in the former and lower in the latter in both regions (Fig. 18).

A common feature in the vertical profile of rain rate over the coastal ocean and mountains are the higher rate over the coastal ocean and lower rate over the mountains up to approximately 5 km AMSL, although the difference is greater over the WG than over the MWC region. There is less difference in conditional rain rate over the coastal ocean and coastal mountains in the lower atmosphere, and the maximum difference is observed at about 4 km AMSL. A similar feature is observed over the central Himalayas, although the differences are smaller, but the stratiform rain type shows the identical trend in vertical profile of the conditional rain rate (Figure not shown). Over the coastal ocean of the MWC region, the lower part of the rain-rate profile in stratiform rain type is nearly constant up to 5 km, similar to the rain-rate profile observed in the central Himalayas. This result indicates a higher depth of moisture in the respective region (the vertical profile of specific humidity revealed higher humidity over the central Himalayas and MWC regions) (Figure not shown). For convective rain, rain rate decreases monotonically with height regardless of topography in both regions. In general, at elevations above 5 km, rain rate in the MWC region is much greater than that in the WG, which indicates that the rain systems are much deeper in the MWC than in the WG. An example of vertical structure of conditional rain rate shown in Figure 19 illustrates good agreement with these features.

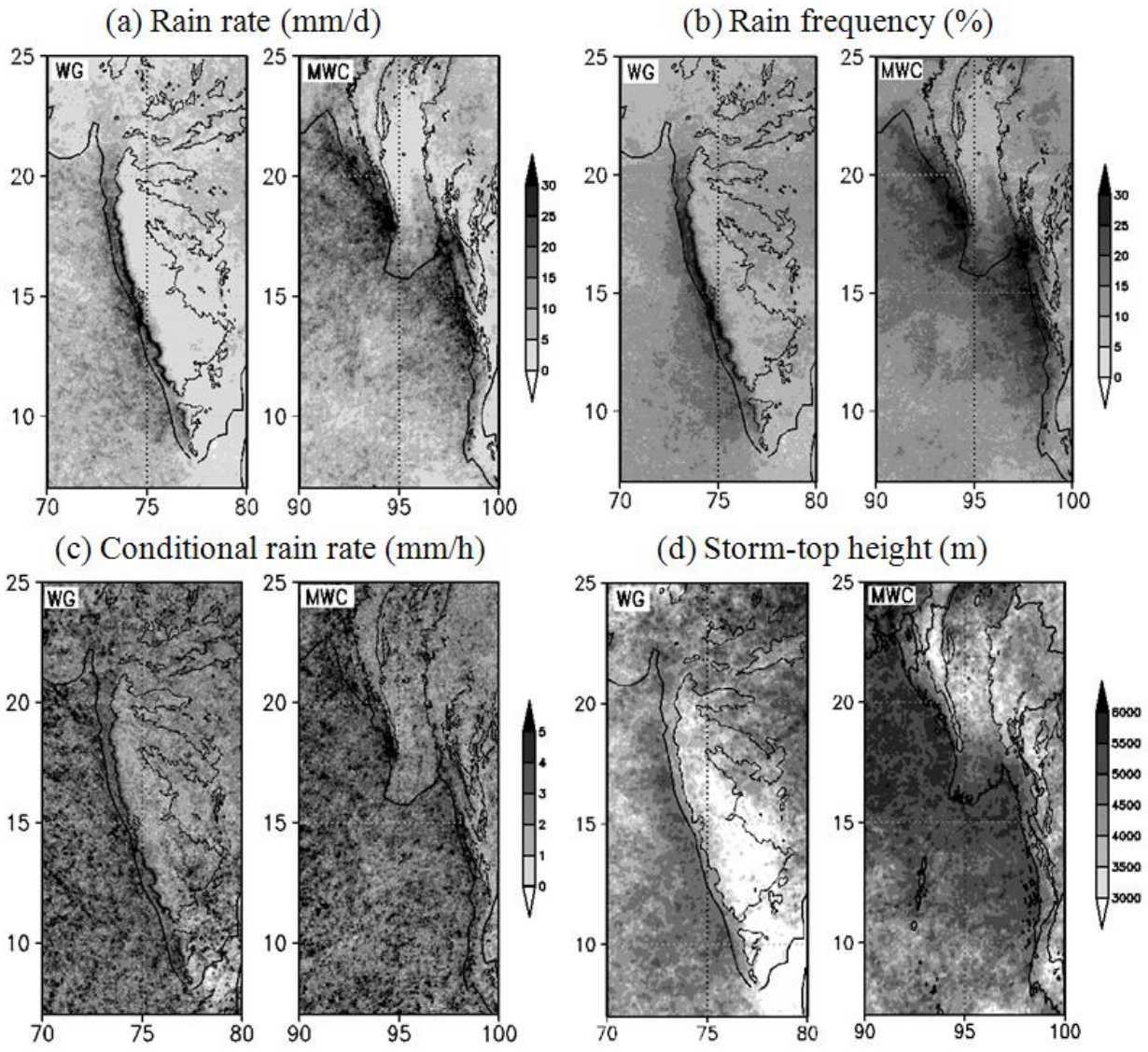

Figure 14. Horizontal distribution of rain characteristics over the Western Ghats (WG, left panel of each figure) and Myanmar west coast (MWC, right panel of each figure) region: (a) rain rate, (b) rain frequency, (c) conditional rain rate, and (d) storm height. Contour line represents 500 m elevations.

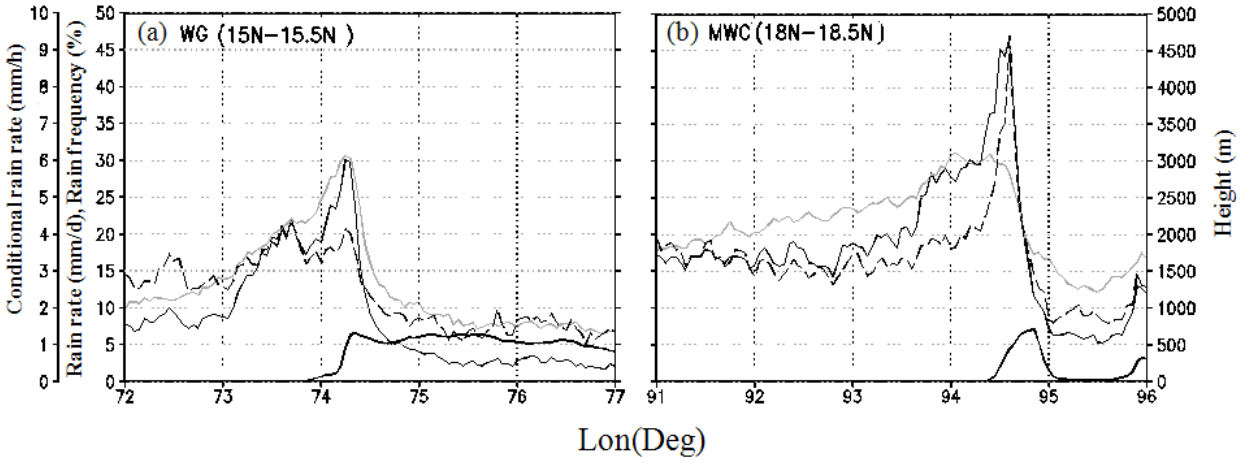

Figure 15. Two sample profiles from west to east of the Western Ghats (a) and Myanmar west coast (b). Heavy solid, thin solid, gray, and dashed lines represent topography (m), daily rainfall total (mm/d), rain frequency (%), and conditional rain rate (mm/h), respectively.

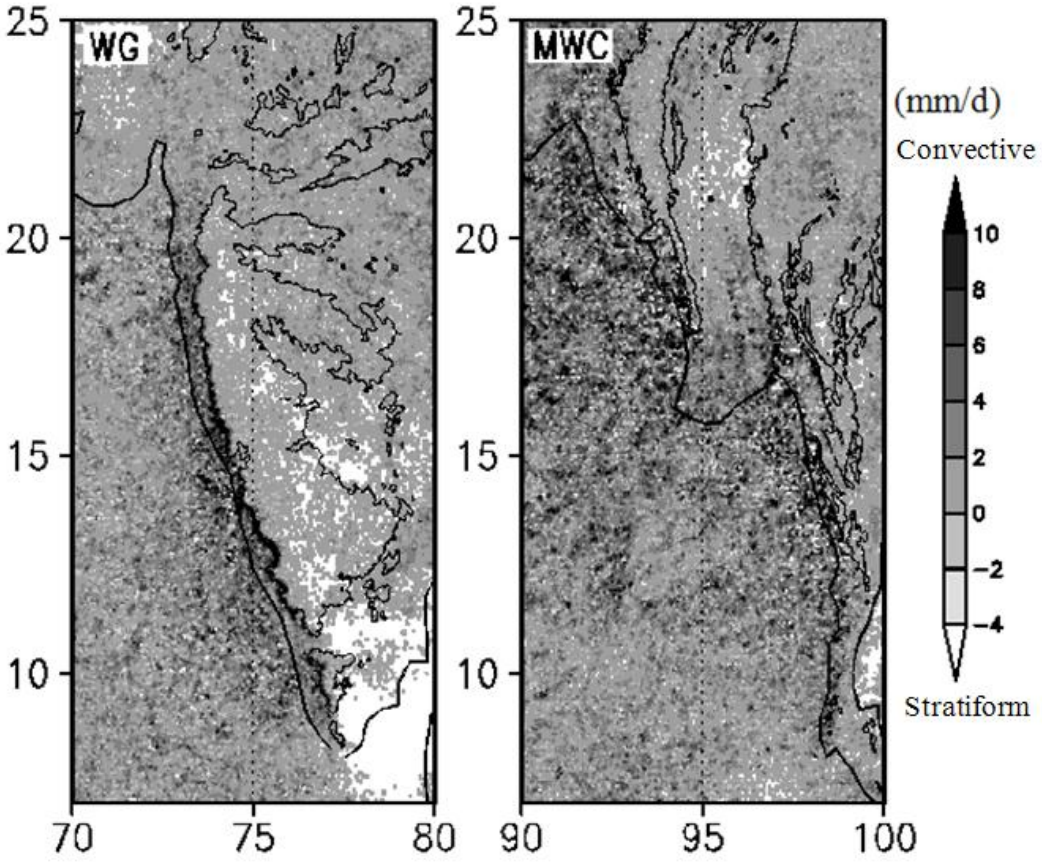

Figure 16. Difference between the convective and stratiform rain amounts for (a) Western Ghats (WG), and (b) Myanmar west coast (MWC). Orographic contour are as in Fig. 2.

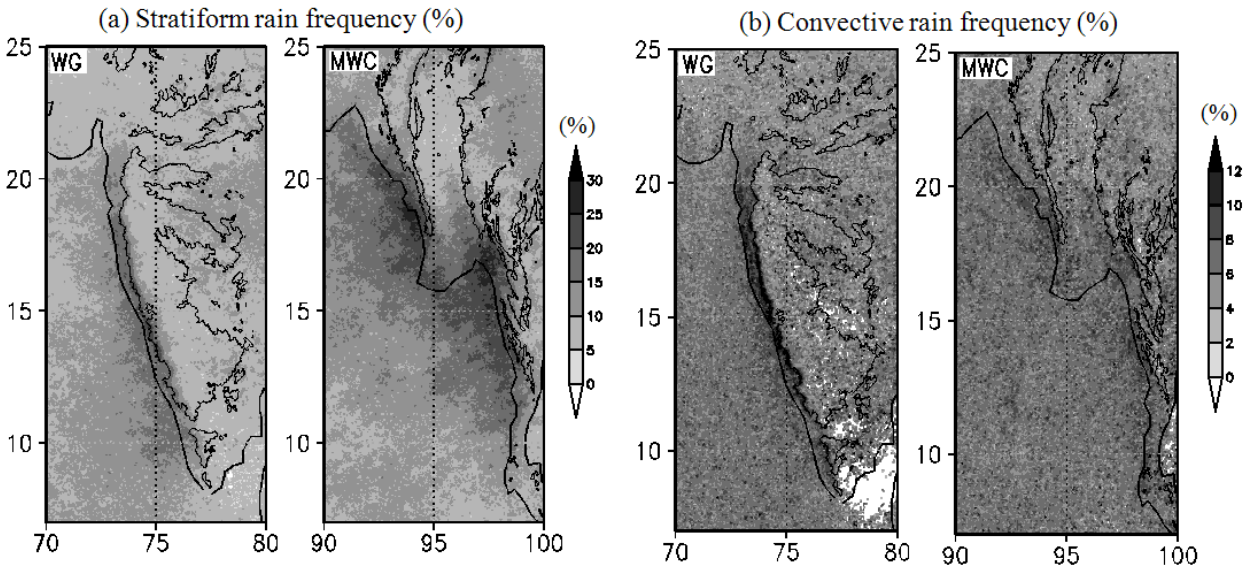

Figure 17. Distribution of rain characteristics over the Western Ghats (WG, left panel of each figure) and Myanmar west coast (MWC, right panel of each figure) region: (a) stratiform rain frequency, (b) convective rain frequency. Orographic contour are as in Fig. 2.

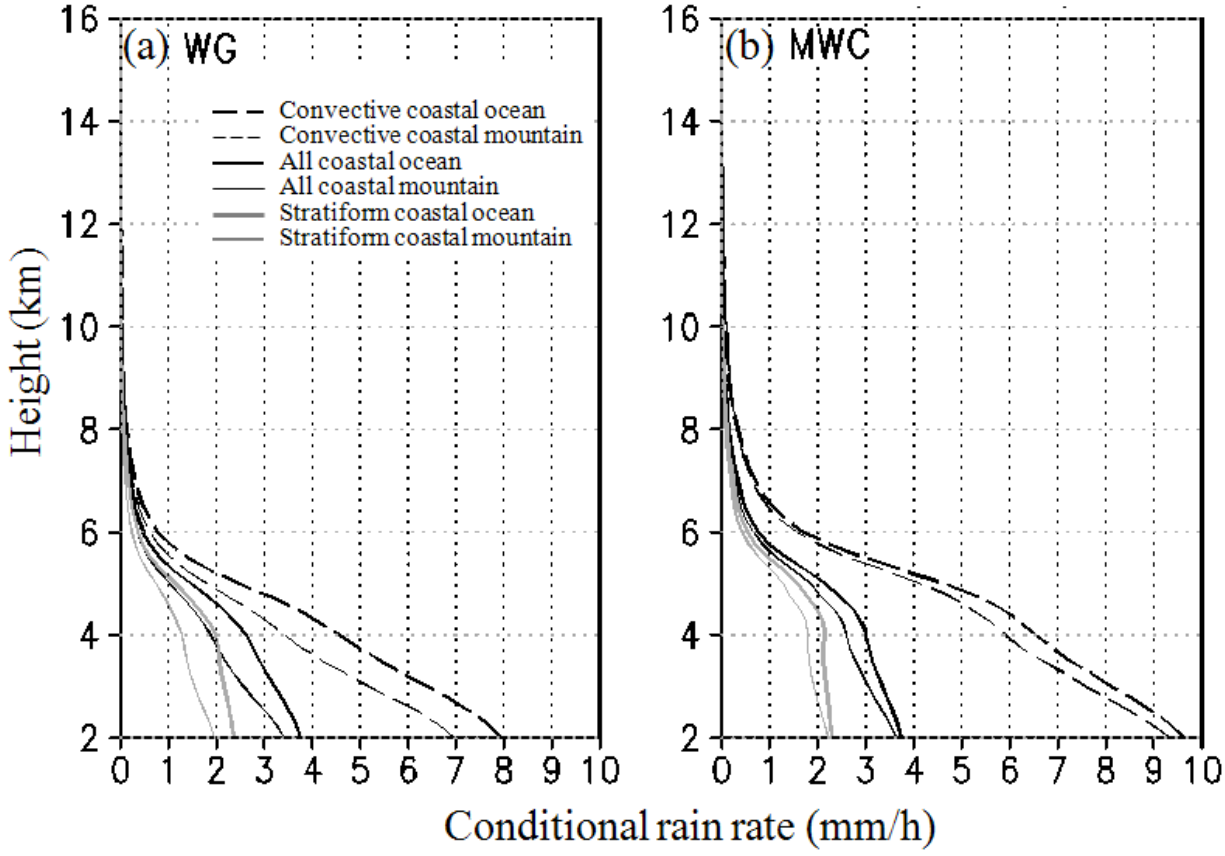

Figure 18. Vertical profile of conditional rain rates over specific region: (a) Western Ghats, (b) Myanmar west coast. Rain rate is averaged over the area shown in Figure 1a.

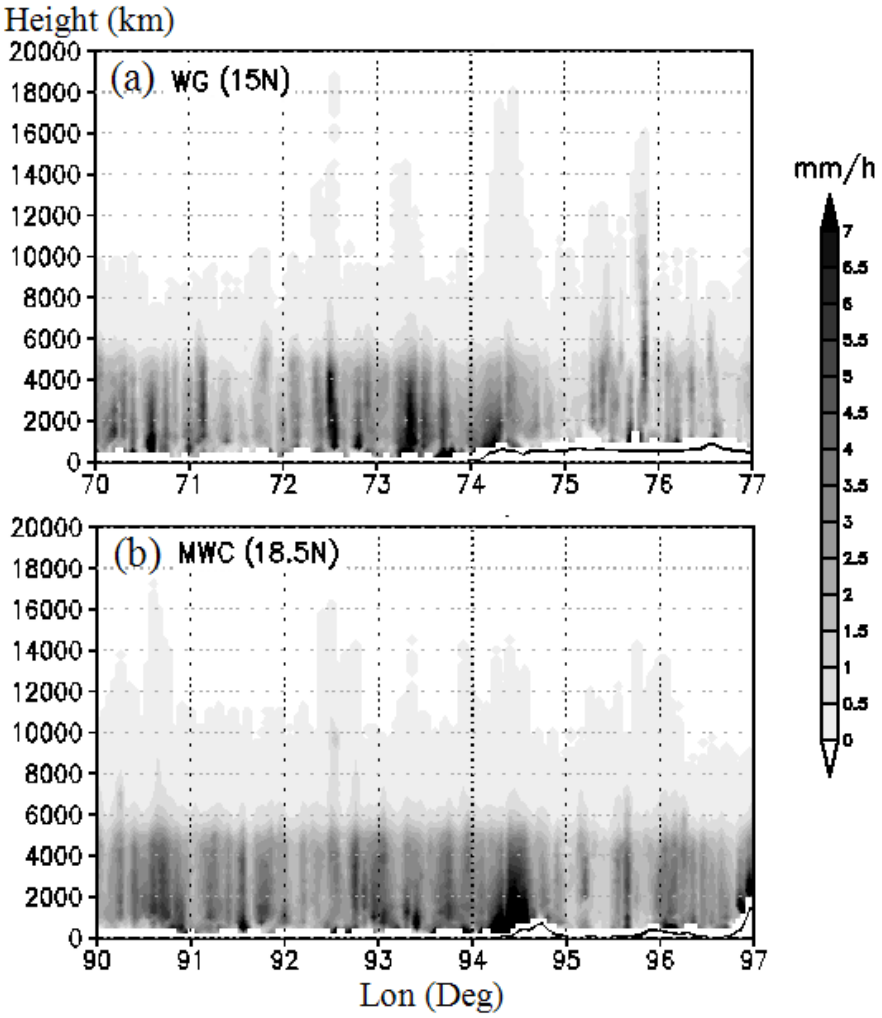

Figure 19. Vertical cross-section of rain rate over the Western Ghats (WG, at 15°N) (a) and over the Myanmar west coast (MWC, 18.5°N) (b). Black line represents east-west topography of coastal mountain ranges.

4.2 Andes ranges

4.2.1 Horizontal distribution

One of the longest and highest mountain ranges in the world, the Andes is a major topographic barrier that modulates the climate of South America. In this region, the distribution of precipitation varies greatly depending on latitude, altitude, and proximity to the sea. The Andes are divided into two subregions on the basis of precipitation characteristics: the central Andes (CA) and southern Andes (SA). Here, we discuss precipitation characteristics over the eastward slopes of these regions.

Figure 20 shows the horizontal distribution of rain characteristics over the Andes region. Along the eastern slope, overall summer season precipitation exhibits a maximum in the higher terrain of the central Andes, and less over the southern Andes (Fig. 20a) as has been previously observed by *Bookhagen and Strecker* [2008] and *Romatschke and Houze* [2012]. Adjacent to the wet Amazon basin, the eastern flanks of the tropical Andes—narrow zones between 500 m and 2000 m in elevation—expedience a large amount of rain rates >10 mm/day (Fig. 20a). *Bookhagen and Strecker* [2008] identified that rain peaks at a mean elevation of 1.3 ± 0.17 km along the entire Andes. Higher terrain (above 2000 m) and the Altiplano receive less rainfall. In contrast to rainfall distribution along the Himalayas, there is no continuous double band of rainfall in the Andes, as this region does not exhibit pronounced two-step topography [*Bookhagen and Strecker*, 2008; *Shrestha et al*., 2012].

The prominent feature of the rainfall characteristics distribution in the Andes region is the rain frequency maxima over the CA regions and high conditional rain rate over the SA regions

(Figs. 20b and 20c). These patterns are almost the same as those observed in the western and central Himalayas. This suggests that rainfall maxima over the central and southern Andes are primarily attributed to rain frequency and conditional rain rate, respectively. Such a correspondence of larger rain rates with rain frequency (conditional rain rate) was also noted in the Himalayan region.

Precipitation characteristics were averaged for each 200-m altitude interval up to 5000 m, for statistical analysis of altitudinal patterns of rainfall. Figure 21 shows the altitudinal variation of these characteristics over the CA and SA regions. The patterns of rain frequency and rain rate are identical, with broad peaks at about 900 m AMSL (Fig. 21a). But conditional rain rates peak at a relatively lower elevation (~500 m AMSL). A similar feature was reported in the central Himalayas (*Shrestha et al*., 2012), where conditional rain rate monotonically decreases with elevation. This result suggests that maximum rainfall over the higher terrain is primarily attributed to rain frequency. Over the SA regions, in contrast, there is a several-hundred-meter elevation lag between rain peak and rain frequency (Fig. 21b). The rain peak, which occurred at 1800 m AMSL, prominently corresponds with intense rain rate.

Figure 22 shows the rain-type distribution over the Andes region during summer. Over the CA, precipitation systems are most stratiform, whereas systems are more convective in the SA regions (Figure not shown). Interestingly, the spatial distribution of frequency and intensity of both types of rainfall are similar, with higher frequency over the CA and higher intensity over the SA. One of the robust features of rain-type distribution is the most-frequent stratiform rain in the central Andes (Fig. 22a), while the highest convective-type conditional rain rate was observed over the SA foothills (Fig. 22b). This feature is consistent with wide convective and broad stratiform echoes in the CA, and wide convective core in the SA foothills [*Romatschke*

and Houze 2010]. In contrast to the central Himalayan region, strong convective rain rate is noticed over the higher terrain of the CA and SA. In general the higher frequencies of stratiform rain are observed in regions with large amount of daily rain totals, particularly over the CA. Overall tendency is consistent with the higher percentage of stratiform rain over CA, and more convective rain over the foothills of SA [*Romatschke and Houze*, 2012].

4.2.2 Vertical profile of rain rate

Figure 23 depicts the vertical profile of conditional rain rate from 2 to 16 km AMSL over the Andes. In both the CA and SA, we examined the vertical profile of rain rate over the area above 500 m AMSL and below 500 m AMSL separately, to understand rainfall-elevation relation ships. At lower altitude, below 4 km, the rain rate in the lower terrain (<500 m AMSL) is more than that in the higher terrain in both the CA and SA. However, differences greater in the CA. At high altitude above 6 km, rain rate in the SA is greater than that in the CA, which means that extremely deep convection dominates more in the SA. This is in good agreement with *Romatschke and Houze's* [2012] findings that precipitation comes primarily from small systems in the SA, which likely represents intense convection during the day. At lower elevations—below 3 km—the rain rate for convective rain decreases, as the height is lower than in the SA. This fact suggests that greater evaporation occurs in the SA.

The vertical structure of rain rate along the east–west cross-section of the CA (13.5°S) and SA (23°S) is shown in Figure 24. Over the CA, the storm top was higher than 14 km above the higher, terrain with intense rain rate in the lower portion of the precipitation column. In general, large amounts of rain observed in higher terrain are associated with deep convection.

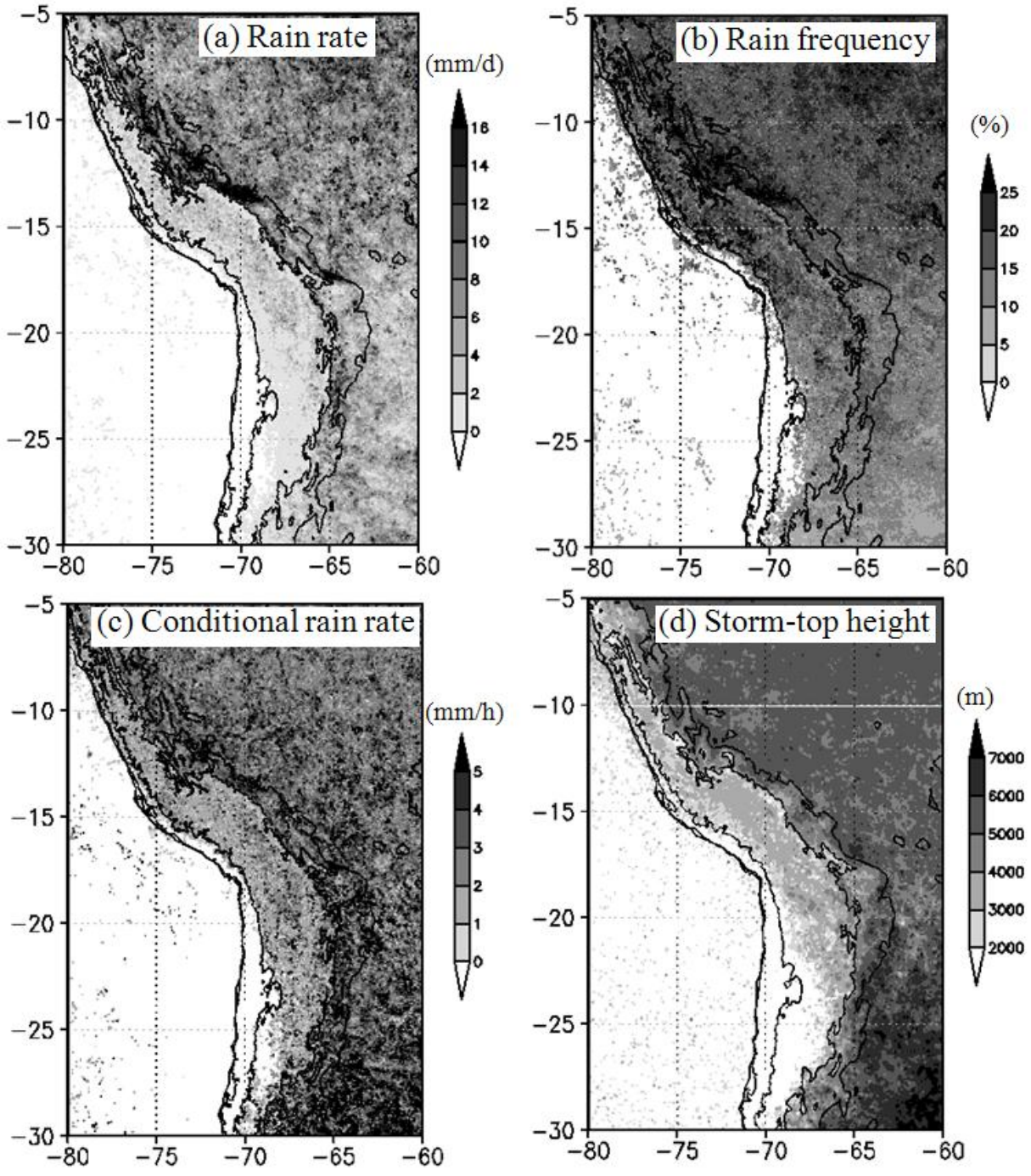

Figure 20. Horizontal distribution of rain characteristics around the Andes: (a) rain rate (mm/d), (b) rain frequency (%), (c) conditional rain rate (mm/h), and (d) storm-top height (m). Contour lines represent 500 and 3000 m elevations.

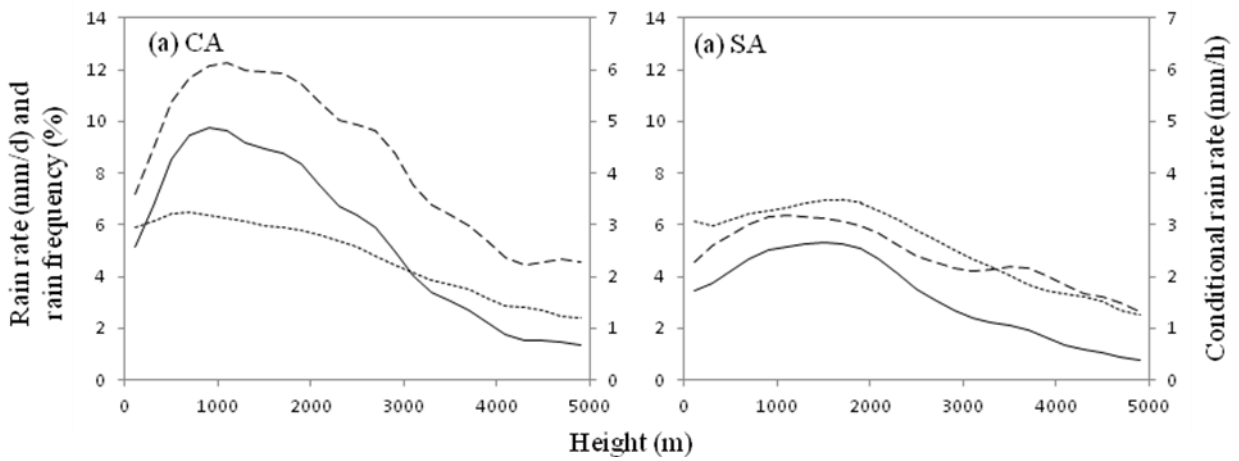

Figure 21. Variation of rainfall characteristics with elevation for (a) Central Andes (CA) and (b) Southern Andes (SA). Solid, dotted, and dashed lines represent daily rainfall total (mm/d), conditional rain rate (mm/h), and frequency of rainfall (%).

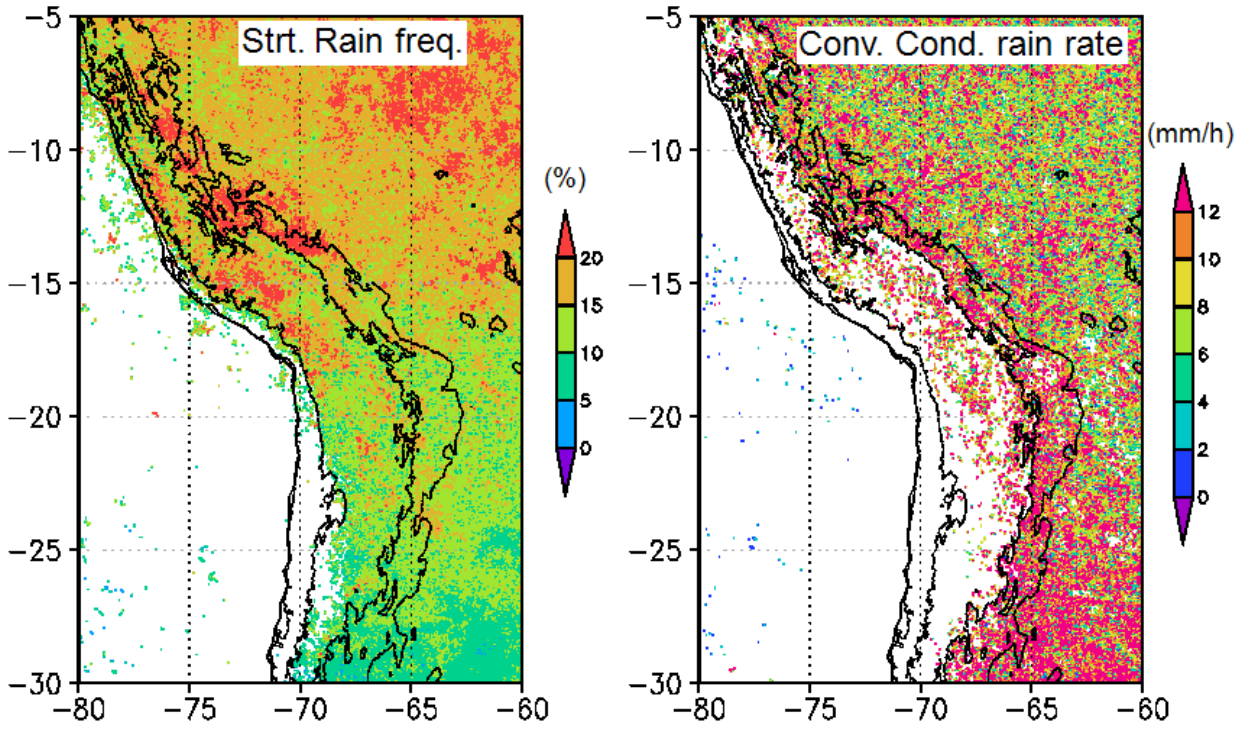

Figure 22. Horizontal distribution of stratiform rain frequency (left panel) and conditional rain rate of convective rain (right panel). Orographic contour are as in Fig. 8.

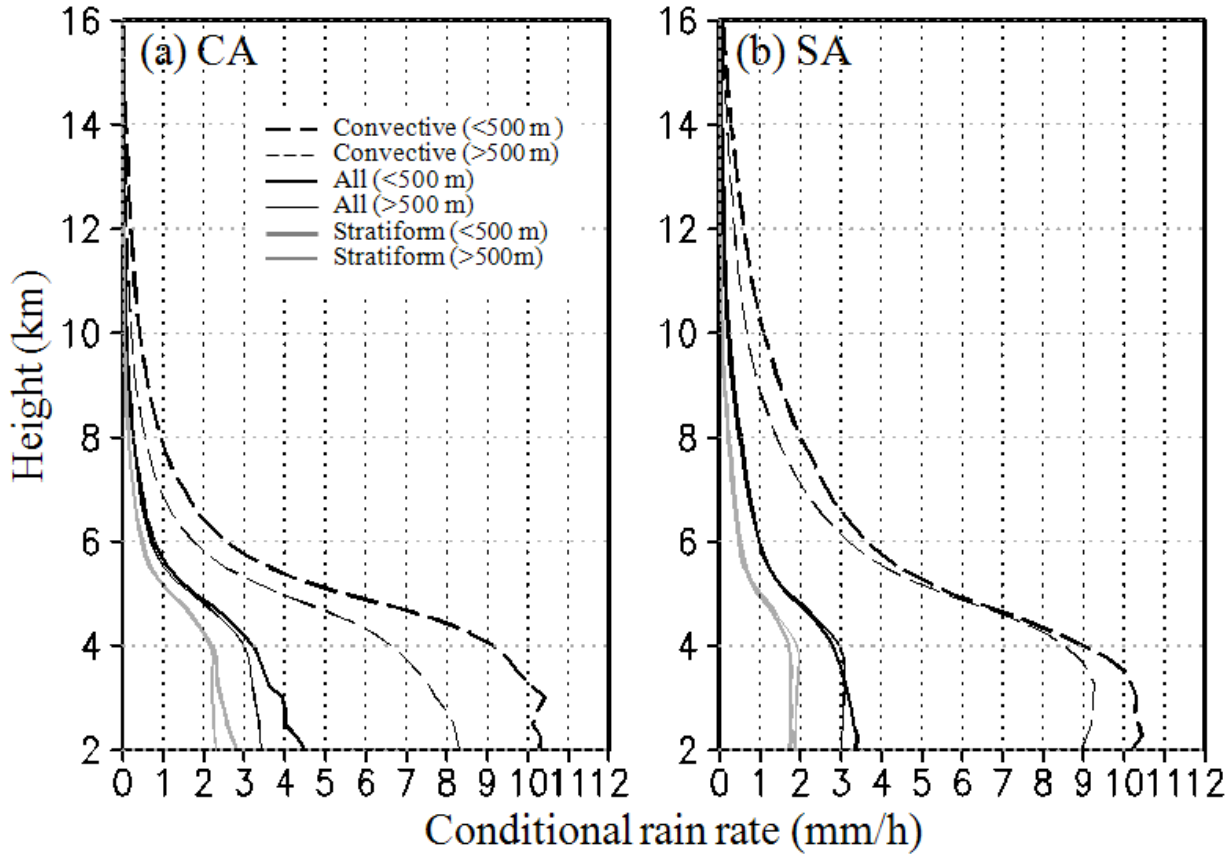

Figure 23. As in figure 6, but for Central Andes (a) and Southern Andes (b). Each region is divided into two subregions: higher terrain (>500 m) and lower terrain (<500 m).

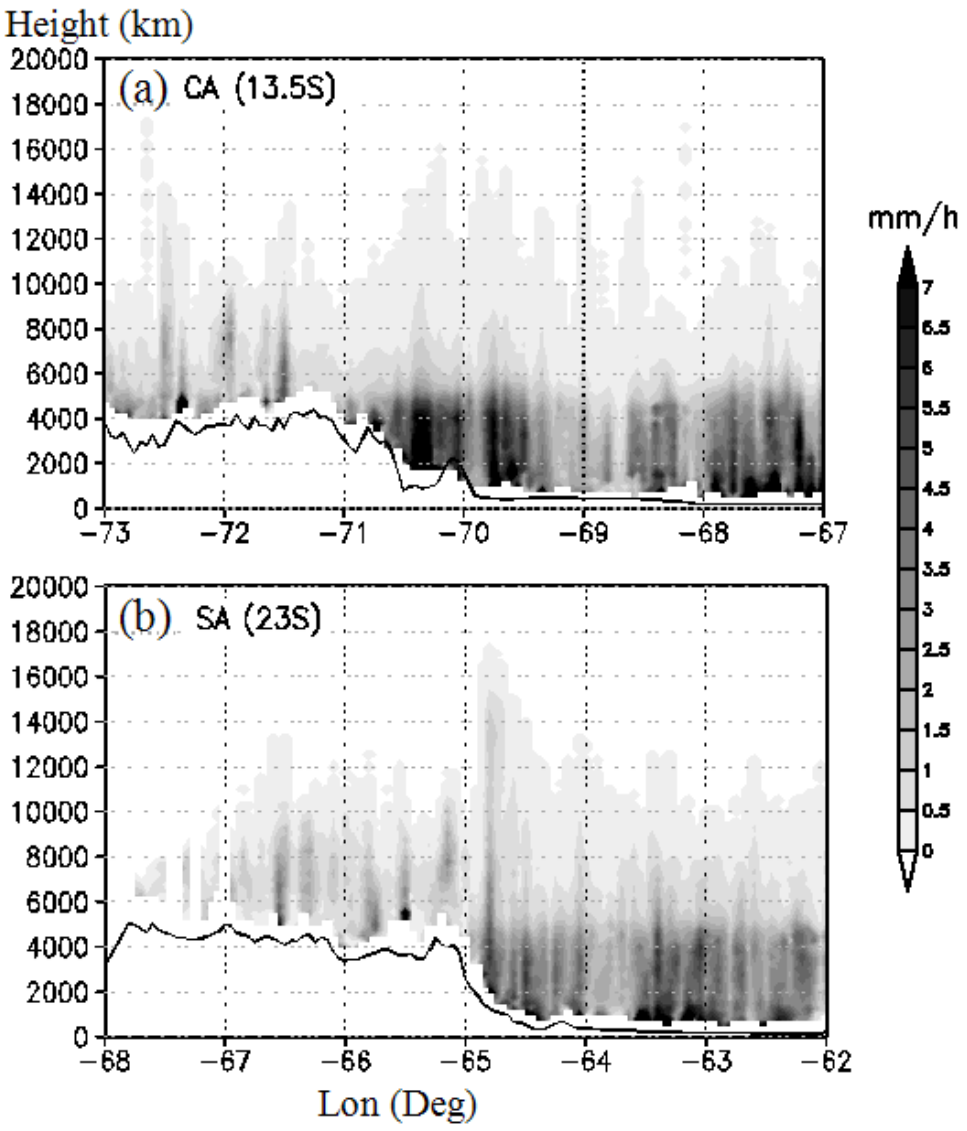

Figure 24. As in figure 7, but for Central Andes (a) and Southern Andes (b).

This is a distinctive feature—different from that noticed over the central Himalayas (*Shrestha et al*., 2012), where maximum rainfall over higher terrain is associated with shallow convection. The highest storm top (above 16 km) occurred over the higher terrain of the SA. Such patterns in storm height suggest extremely deep convections. A similar feature was observed in the northwestern Himalayas [*Houze et al*., 2007, *Medina et al*., 2010].

4.3 Atmospheric Condition

Here we examine atmospheric stability because it provides us an interpretation of the precipitation characteristics. As it is done on the central Himalayas (Sub-section 3.6), we used climatological variables (temperature, moisture, wind) that are available at climatological and individual scales. Evaluating the horizontal and vertical structure of equivalent potential temperature (θ_e) is an important meteorological variable for understanding the atmospheric instability. The structure of the circulation field during the summer monsoon,from JRA-25 reanalysis, is shown in Figure 25. Although the general patterns are remarkably similar between the two coastal regions, there are clear differences in horizontal wind direction and θ_e (Figs. 12a and 12b). The westerly wind is prominent over the WG region while MWC regions are dominated by strong southeasterly winds. Over the WG region, the strong, moist westerly wind from the Arabian Sea strikes perpendicularly to the hill. The difference in θ_e between two pressure levels (925-600 hPa) shows slightly more atmospheric instability in the MWC region, and higher θ_e is observed there as well. The higher specific humidity (above 16 g/kg at 900 hPa) over MWC compared with WG (below 16 g/kg at 900 hPa) confirms that the higher θ_e over MWC is due to a large amount of water vapor in the atmosphere.

The horizontal patterns of atmospheric variables in the Andes region are shown in Figure 25. The summertime low-level (925 hPa) wind pattern contains several features that are key to understanding the precipitation mechanisms. Along the eastern foothills of central Andes, northerly component winds parallel to the mountains and advects moisture from wet Amazon to the southern Andean foothills (Fig. 25a). *Romatschke and Houze* 2012 explained that the strength of these northerly wind connected to the passage of synoptic-scale disturbances has a profound role on the location of extreme convection around the Andean regions. In the seasonal mean of surface wind, heating over the Andes forces the low-level wind upslope, which converges over the mountains (Figure not shown). This feature is clearer in the SA than CA. There is remarkably similar feature in θ_e between CA and SA at 925 hPa. The smaller difference in θ_e between 925 and 600 hPa indicates more stable atmospheric conditions over the CA (25b). In contrast, a strong convective instability is apparent over the SA, although the θ_e is relatively small. The horizontal wind shows distinct features between the lower and higher elevations, i.e., low-level northeasterly moist flow from the wet Amazon basin, and westerly wind flow in the upper atmosphere. These tendencies are conducive to deep convection related to well-known capping mechanisms as explained previously (*Rasmussen and Houze*, 2011).

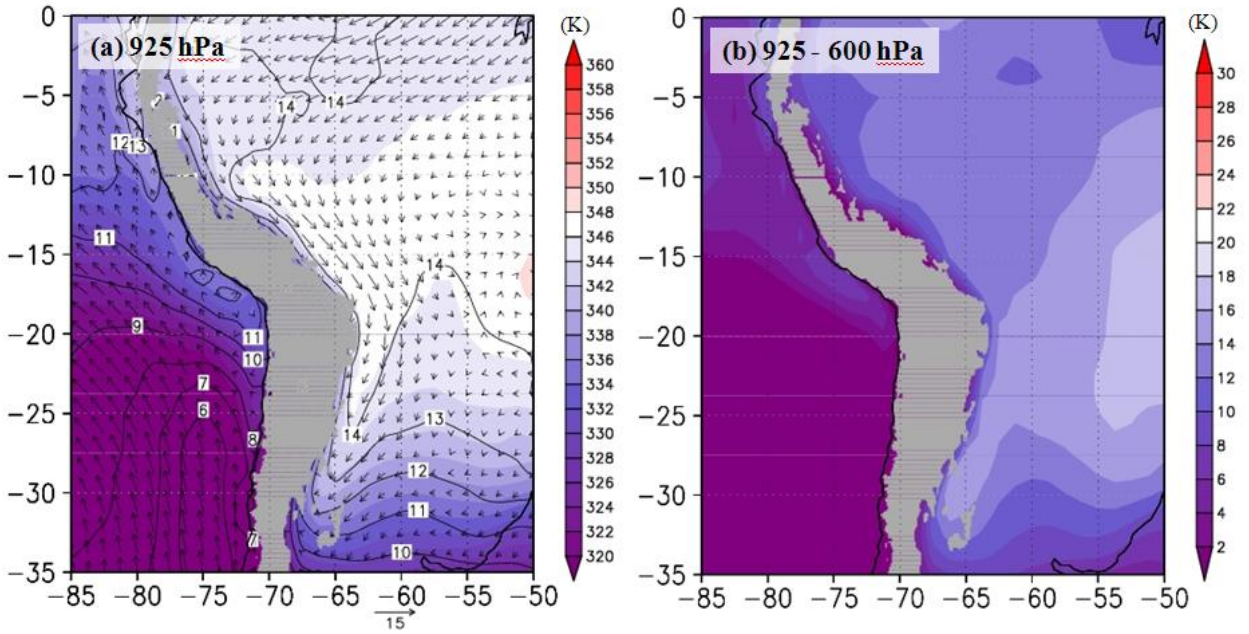

Figure 25. JRA-25 climatology of equivalent potential temperature (K; color shaded), winds (m/s; black arrows), and specific humidity (g/kg, black contours) at 925 hPa (a), and difference in equivalent potential temperature between two pressure levels (925 and 600 hPa) (b), for South American summer (December–February). Gray shading represents topography above 800 m (~925 hPa).

5. Discussions

In this study, we have compiled more than a decade long precipitation data at very high spatial resolution (0.05° × 0.05° and 0.1° × 0.1°) obtained from the Precipitation Radar aboard TRMM. Spatial distribution of summer precipitation characteristics over the central Himalayas, the Andes and the western coastal mountainous area of South Asia (WG, and MWC), specifically focusing on topographic impact, is characterized in terms of rain frequency, intensity, type, and their vertical structures. In addition, precipitation characteristics during pre-monsoon, and active and break summer monsoon were investigated for the central Himalayan region. The atmospheric condition is also analyzed in terms of equivalent potential temperature to determine the mechanisms involved in the development of spatially distinct precipitation systems. In general, this study presents a comparative analysis of precipitation mechanisms over the rugged topography under moist and rather dry atmospheric conditions.

The temporal resolution of TRMM PR does not provided continuous observations, but rather yields one to several snapshots per day depending on latitude. Despite the sampling errors are still significant even after a decade-long data collection, averaged value over the whole recorded period provided a reasonable estimate of rainfall distribution over the complex terrain of the study areas. In recent research, *Nesbitt and Anders* [2009] indicate that the current climatology is sufficient to accurately capture steep rainfall gradients. The PR-observed precipitation features have shown good agreement with previous studies.

5.1 Himalayan and Andean regions

The north–south topographic gradient in the Himalayas is extremely high, which can cause strong orographic forcing. Thus, variation in rainfall characteristics between the southern

Himalayan foothills and higher altitudes could be pronounced. Along the Himalayas, distinct topographic patterns exist, with the eastern and western Himalayas characterized by steadily rising one-step topography, and the central Himalayas by two-step topography [*Bookhagen and Burbank*, 2006, 2010]. Such topographic features reflect distinct spatial patterns of rainfall in the eastern (EH), central (CH), and western Himalayas (WH), and these patterns are more pronounced in JJA than in MAM. The EH is situated near a major moisture source, whereby low-level moisture flow collides with steadily rising one-step topography to produce a low-altitude rainfall peak (below 1,000 m above MSL). *Romatschke and Houze* [2011a] suggested that the fraction of convective rain in small systems is lower in the EH which is consistent with the large stratiform regions that occur along the eastern Himalayan foothills [*Houze et al*., 2007]. One of the reasons for the high rainfall at the mountain front is that it is a high-relief area, which prevents rainfall from penetrating to higher altitudes [*Bookhagen and Burbank*, 2010]. The WH, far from the moisture source, where rainfall is concentrated at higher altitudes has tall storm-top height. A large fraction of rainfall in small rain systems in this region is convective in nature [*Houze et al*, 2007; *Romatschke and Houze*, 2011a]. In addition, the highest rates of lightning activities found in this area suggest deep convection [*Bookhagen and Burbank*, 2010]. Our main focus in the Himalayan region is CHR, where double peaks of rainfall maxima parallel to the mountain ranges have been observed.

A schematic of rainfall processes over the southern slopes of the Himalayas (focusing on the CHR) during MAM and JJA (including active and break periods) is presented in Figure 26. Once precipitation systems begin, they tend to be more intense during MAM (Fig. 26a) than JJA (Fig. 26b). This is consistent with more intense lightning activity during MAM than JJA over the CHR [*Bhatt*, 2005; *Barros et al*., 2004)]. During MAM, the CHR is characterized by a dry

atmosphere with strong dry northwesterly winds. This generally does not favor generation of precipitation systems. Despite the unfavorable synoptic conditions, rainfall is yielded from a limited amount of locally enhanced convective activity. The intense rainfall that occurs during MAM over the SH is due to strong AI (Figs. 7a and 13a), that is, once convection starts, it is likely to strengthen. More precipitation systems develop over the LH than over the SH, resulting in a higher rain rate in the LH. This is probably orographically enhanced convection. In other words, strong AI triggers deep intense rain systems near the SH, whereas orography triggers frequent rain systems over the higher Himalayas. The deep convection over the SH may help moisten the middle layer and reduce atmospheric instability. During JJA, systems are less convective but more persistent with higher mean rain rate. Such rainfall characteristics may suggest that precipitation systems develop in humid and more stable environments. The important characteristics of rainfall distribution during JJA over the southern slope of the CHR are as follows: the SH peak is a result of intense rainfall, and the LH peak of persistent rainfall. This fact suggests different rainfall processes over the SH and LH. The frequent lightning events in the lower elevation areas also support the assertion that rainfall over these areas occurs with stronger convection [*Bookhagen and Burbank*, 2010]. Precipitation systems near the SH may be categorized by abundance of water vapor in the lower atmosphere, while higher Himalayan precipitation systems involve more mechanical processes (i.e., forced lifting due to steep Himalayan slopes). These features are similar to those in MAM, but the precipitation systems are generally weaker.

As explained in subsection 3.5, the active-phase rainfall is concentrated around SH (Fig. 26c); it is first attributed to conditional rain rate, followed by rain frequency. Despite the lower rain-top height (~8 km), intense rainfall appears up to 6 km elevation (Fig. 10a). This means that

abundant moisture supply in the lower atmosphere favors easy triggering of convection, when the moisture encounters low frontal mountains ranges; *Houze* [2012] explained such triggering over the foothills ahead of the main mountain barrier. The moisture convergence during active periods is associated with the shifting of the trough line close to the foothills of the Himalayas. Conversely, break periods are characterized by relatively lower moisture content, steady easterly winds and higher solar radiation as the monsoon trough shifts southwards. Such conditions generally do not favor ample rising of dry air to reach the lifting condensation level (LCL). Thus, rainfall systems rarely propagate over low land. Precipitation systems in break periods exist under rather unstable atmospheric conditions, enhanced by strong solar heating. Despite the lower moisture content in the air, the major mountain barrier provides a strong trigger to initiate convection over higher altitude regions (Fig. 26d).

Over the Andes, striking spatial gradients in the climatology of precipitation that depend on latitude and altitude were found (Figs. 27a and 27b). It is evident that most of the rainfall concentrated over the higher terrain of the eastern slopes of Andes. The precipitation systems in the central and southern Andes are generally characterized by frequent stratiform rain and occasional intense convective rain, respectively. The precipitation systems in the CA are mostly medium-to-large in horizontal extent, and are associated with large stratiform regions [*Romatschke and Houze*, 2010, 2012]. This suggests that, similar to the central Himalayas, precipitation systems develop in humid and stable atmospheric conditions. But unlike the central Himalayas, deeper systems were formed over the higher terrain compared with the lower terrain. A lower specific humidity observed over this region could be responsible for these distinct features. Thus, we suggest that the steep slope of mountains provides forced lifting when low-level, unsaturated moist air is flowing over the terrain. Conversely, the higher terrain of the SA is

characterized by strong convective instability with less-humid conditions. Here, the precipitation system is mostly characterized by horizontally small but extremely deep convective cores [*Romatschke and Houze,* 2010, 2012]. In the SA, systems of an intense convective nature form when low-level flow from the wet Amazon and/or Atlantic region is capped by mid-level dry westerlies [*Rasmussen and Houze,* 2011].

One of the interesting findings is that the rain-conditioned rain rate simply decreases with altitude regardless of the rain amount in wet seasons, while the rain frequency peaks near an elevation of approximately 2,100 m (Fig. 6). How can this result be understood? One idea is that the rain is caused by forced lifting. When humid air collides with the mountain slope, it is lifted along the slope. The air temperature decreases as the air lifts and, at the LCL, condensation occurs and rain begins. If the lifting continues, the rain persists. In this case, the amount of rain could simply be estimated from the change in saturation water vapor pressure with temperature. Figure 28 shows the amount of condensation relative to altitude on the basis of the hypothesis that the air is saturated at the beginning. The saturated air produces rain in proportion to the lines in the figure. When the colliding air is not saturated by water vapor, condensation will not appear below the LCL. In this case, no precipitation appears below the LCL. Actual relative humidity varies, as does the LCL. Thus, the amount of rain after averaging may peak at an elevated level instead of ground level. On the other hand, if the lifting is nearly the same under wet or dry conditions, the rain-conditioned rain rate may be the same. Thus, the rain-conditioned rain rate monotonically decreases with elevation independently of the rain total, but the frequency of rain peaks at a specific level.

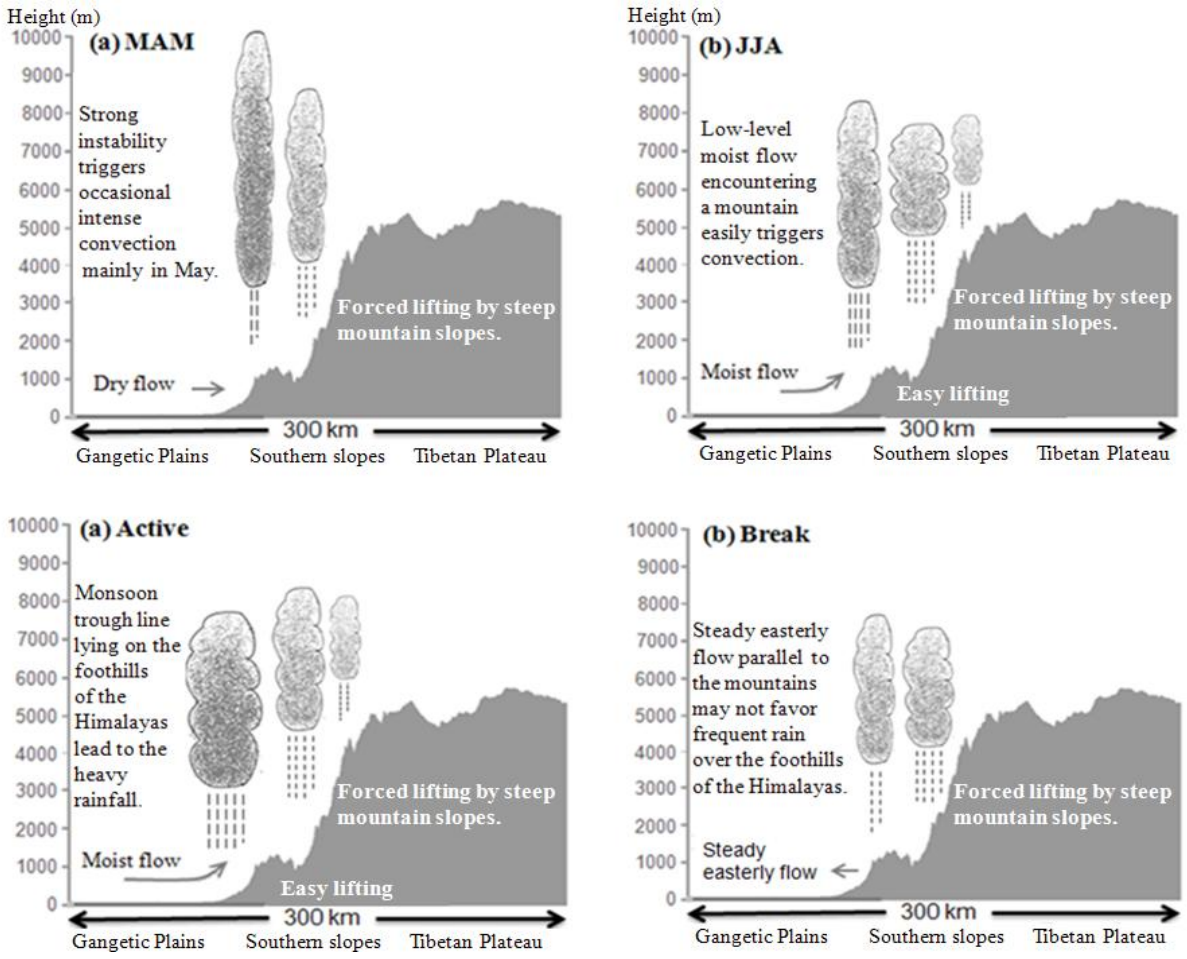

Figure 26. Schematic illustrations of spatiotemporal variation in rainfall for (a) pre-monsoon, (b) summer monsoon (JJA), (c) active monsoon, and (d) break monsoon.

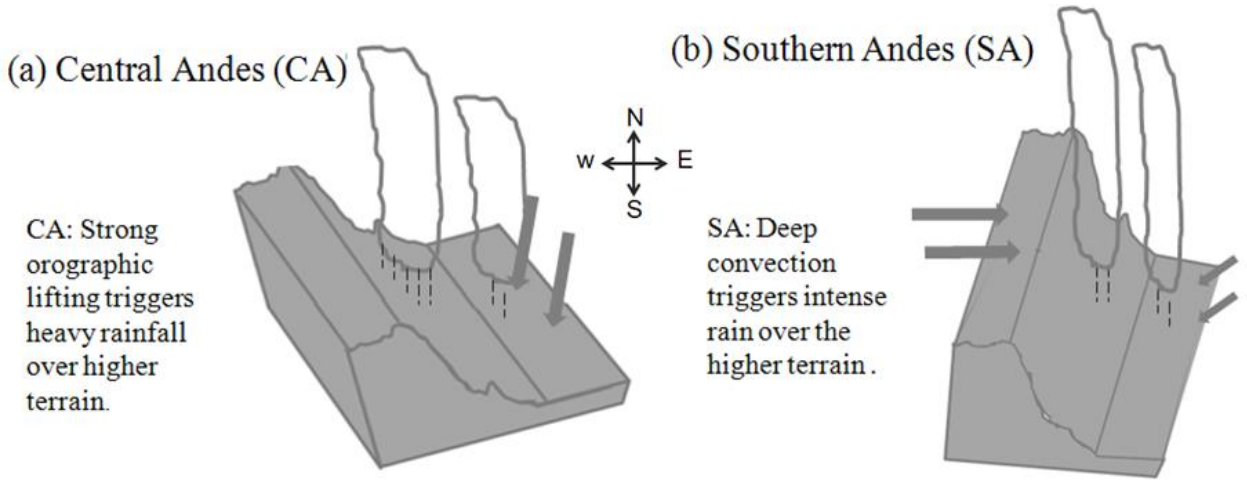

Figure 27. Schematic diagram of the mechanisms for the precipitation variability over the central Andes (a), and southern Andes (b).

Height (km)

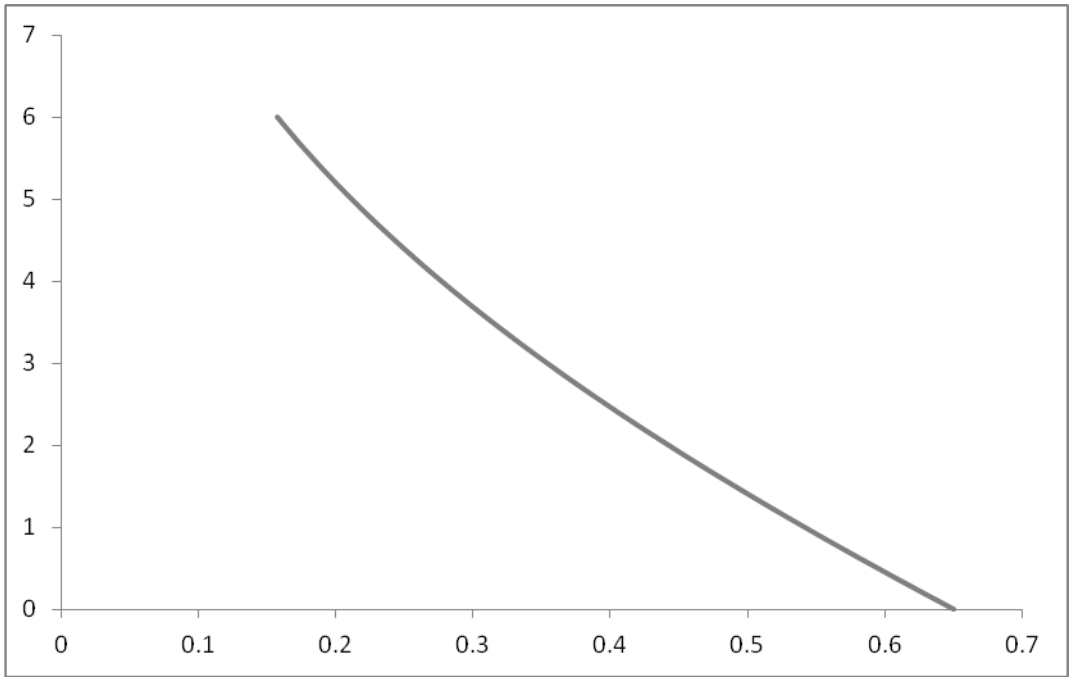

Condensation (g/kg/100 m)

Figure 28. Amount of condensation for 1-kg air by steady lifting. The temperature lapse rate is assumed to be 6.5°C/km; air temperature and air pressure are 30°C and 1013 hPa, respectively, at 1-m height.

5.2 Coastal regions

Previously, we showed a spatial correlation among topography, rain frequency and intensity, which determines the position of the double rainfall band in the central Himalayan region [*Shrestha et al*., 2012]. Investigation in both coastal and continental mountainous regions of south Asia and the Andes also revealed a correlation between elevation and the locations of maximum rainfall. However, the correlation varies greatly from place to place. A schematic of summer monsoon rainfall mechanisms in the study area is shown in Figure 29. Over the coastal regions, the heaviest precipitation zone locates primarily over the western slope of the coastal mountains and extends westward over the oceans. Primary factors determining the peak rainfall over the coastal mountains and ocean are rain frequency and intensity, respectively. A rainfall maximum that strongly increases in frequency as elevation increases is indicative of orographic anchoring. A weak signature in diurnal cycle of small and medium systems in the coastal mountains of WG and MWC, which plays a dominant role in total rainfall over the WG and a significant role over the MWC [*Romatschke and Houze*, 2011a], thus suggesting that an orographic response to the prevailing low-level southwesterly monsoon flow is a key factor in addition to the land-ocean contrast. As the southwest monsoon impinges on the narrow coastal mountains of the west coasts of India and Myanmar, moisture-laden air is forced to rise and causes frequent convections on the upwind sides. In addition to the orographic lifting effect as a dynamic barrier to the prevailing winds, coastal mountains play an important role in a strong diurnal cycle of convection over the coastal ocean and surrounding lands due to diurnal thermal forcing [*Xie et al*, 2006]. Intense rainfall associated with taller storm-top heights over coastal oceans is more likely because of the strongest morning convergence, when onshore progression of monsoon flow along the coast is slowed down by cooling over the continent.

There is a substantial difference in precipitation mechanisms between WG and MWC (Figs. 29a and 29b). The systems in the WG region tend to be more convective compared to those in the MWC, although the storm-top was much higher in the MWC regions. *Romatschke and Houze* [2011a] also identified that most systems in the WG region were small or medium, while systems in the MWC were mostly large in size. They further reported a great amount of shallow, nonextreme convection over the WG region, which does not develop into a large system. These differences could be related to prevailing moisture and sea-surface temperature conditions over these regions. The vertical structure of equivalent potential temperature confirms that the lower atmosphere over the MWC is more humid than that over the WG region. Insufficient moisture does not favor growth of large-scale precipitation systems over the WG region. However, the strong, moist westerly wind from the Arabian Sea strikes perpendicularly to the hills in a roughly in a north-south direction, and rises vertically during the summer monsoon causing very heavy rainfall on the windward side. In contrast, sufficient humidity, high sea-surface temperature, and consequent orographic lifting help to generate large precipitation systems in MWC regions. Several researchers have suggested that the Bay of Bengal depression favors the formation of mesoscale convective systems over the Bay of Bengal [*Houze et al*., 2007; *Romatschke et al*., 2010].

Overall, this study presents a comparative analysis of precipitation mechanisms over the rugged topography under moist and rather dry atmospheric conditions. Evaluating the precipitation characteristics around the mountainous regions in South Asia and South America indicates that the low-level moisture condition is a key factor to determining the precipitation mechanisms around the mountainous regions. When atmosphere is sufficiently humid, wide area precipitation systems are easily triggered under relatively stable atmospheric conditions. Thus,

large amount of rainfall occurs over the low-altitude areas and decreases with altitude. Precipitation mechanisms during active period in the central Himalayas, coastal mountainous region of MWC, and CA regions are an example of such mechanisms. However, each region has its own circulation characteristics and thermodynamic environments. On the other hand, atmosphere is rather unstable under less humid atmospheric conditions, resulting in intense rainfall over a certain altitude. Such features are observed in the central Himalayan region during break monsoon and pre-monsoon over the central Himalayas, WG and SA regions. Diurnal cycle of atmospheric system has also important role on precipitation mechanisms over the mountainous environments, be it mountain/valley or land/ocean breeze, A climatological-dynamical analysis by *Bhatt and Nakamura* [2006] suggests thermally induced up-valley wind during day time triggers ridges convection, while confluence between down-valley wind and large-scale monsoon flow during night time triggers moist convection over the southern foothills. Study of precipitation mechanisms over complex terrain—specially those based on rain frequency and conditional rain rate provided by the TRMM PR alone—is still incomplete. This study indicates some of the possible precipitation mechanisms that occur over the mountains. Ultimately, advanced fine-scale models will be necessary to improve our understanding of the precipitation characteristics over complex mountainous terrain.

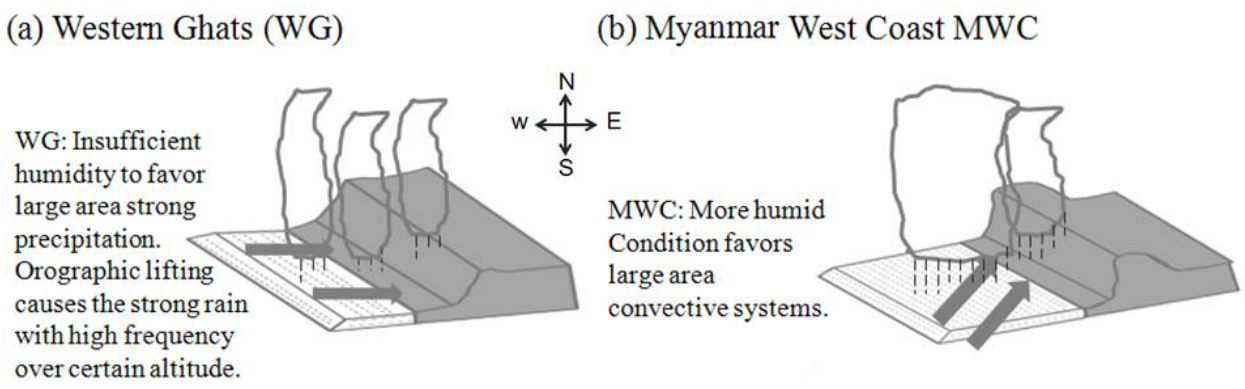

Figure 29. Schematic diagram of the mechanisms for the precipitation variability over the Western Ghats (a), and Myanmar west coast (b).

6. Conclusions

This study focused on spatial variability of summer precipitation characteristics, with a particular focus on their relationship with elevation, over the complex mountain terrains; The Himalayas, the Andes, and the mountainous western coast of India and Myanmar. Despite the significant uncertainty due to poor temporal sampling of TRMM PR, decade-long climatology of precipitation revealed several interesting features, which are comparable to previous research.

Over the central Himalayas, the analysis of rainfall characteristics showed different scenarios for the spatiotemporal distribution of rainfall during the summer monsoon and pre-monsoon periods. There is an increase in peak rainfall over higher altitudes, and a decrease over the frontal low-altitude region, during the pre-monsoon season. A case study in 2004 revealed that a few intense rainfall events dominate pre-monsoon rainfall and are associated with strong atmospheric instability. During the summer monsoon, two high-rainfall zones clearly appeared over the southern slope of the central Himalayan region. The frontal high-rainfall zone coincided with the Sub-Himalayas (~500–700 m AMSL) and the inner, rather broad high-rainfall zone coincided with the Lesser Himalayas (~2,000–2,200 m AMSL). The southern slope of the Sub-Himalayas received high rainfall as a result of fewer heavy rainfall events, while the Lesser Himalayas received high rainfall as a result of the high frequency of relatively weak but persistent rainfall. It is suggested that precipitation systems are mostly triggered by strong atmospheric instability in the pre-monsoon season, while sufficient moisture induced by low-level southeasterly flow triggers persistent rainfall during the summer monsoon season.

In addition, an inspection of intraseasonal variability in rainfall during the mature monsoon season revealed that active-phase rainfall was dominant over the slopes of the frontal low

mountains; however, break-phase rainfall was dominant in total monsoon rainfall over the Lesser Himalayas. High temperatures and strong low-level moisture flowing over low elevations may create favorable conditions to initiate convective rainfall. Although such conditions do not appear over higher terrain, forced lifting due to steep orography favors persistent rainfall.

Over the eastern slopes of the Andes, striking spatial gradient, depending on latitude and altitude, in climatology of precipitation characteristics was found. The zone of rainfall maxima observed over the higher terrain of the central and southern Andes is attributed to rainfall frequency and intensity, respectively. In the foothills of the central Andes, a persistent rain system occurs when moist low-level flow is lifted. In contrast, a relatively dry atmosphere and steep mountain slopes favor deep convection in the southern Andes foothills.

In the both coastal regions WG and MWC, a maximum rainfall along a tight line on the upwind side of the coastal mountains is primarily attributed to rain frequency. However, intense precipitation was observed over the offshore regions. Compared with the WG, deeper and large-scale precipitation systems develop over the MWC, producing more-intense rainfall. It is suggested that insufficient humidity does not favor large scale convection over the WG, and the atmosphere is sufficiently moist over the MWC.

This study suggests that the amount of moisture in the lower troposphere is one of the primary factor which determines the precipitation mechanisms over the mountainous regions. Abundant moisture supply in the lower atmosphere favors persistent rainfall over the low-altitude areas, while intense rain peaks at certain altitude when relatively less humid air is lifted over the steep slopes of the mountains. Further quantitative and qualitative investigations are needed to clarify these results.

Acknowledgements

The author would like to express his sincere gratitude to Prof. K. Nakamura for his constant support, superb guidance and encouragement throughout the course of this work. He is grateful to Prof. H. Uyeda, Assoc. Prof. H. Masunaga for thoughtful comments and suggestions. The author owes a deep sense of gratitude and sincere thanks to Dr. P. Singh , Dr. M. L. Shrestha, Mr. T. Adhikari for their inspiration and invaluable help. Special thank is extended to Ms. T. Tanaka, Dr. C. Lim, Mr. K. Toyoshima and S. KC for their incredible help. He is also thankful to Dr. F. A. Furazawa, Dr. M. Nishikawa, Dr. H. Minda and all staffs of the Hydrospheric Atmospheric Research Center, Nagoya University, for their generous help. Thanks are also due to all members of the satellite meteorology laboratory and the cloud and precipitation climatology laboratory.

Sincere thanks go to the Ministry of Education, Culture, Sports, Science, and Technology, for providing me financial support through Monbukagakusho scholarship. The author would like to thank the Japan Aerospace Exploration Agency (JAXA) for providing TRMM datasets.

Last but not least; he would like to thank his parents, all his family members, for their love and endless supports.

References

Anders, A. H., G. H. Roe, B. Hallet, D. R. Montgomery, N. J. Finnegan, and J. Putkonen (2006), Spatial patterns of precipitation and topography in the Himalaya, *Spec. Pap. Geol. Soc. Am*., 398, 39–53.

Annamalai, H., and J. M. Slingo (2001), Active/break cycles: Diagnosis of the intraseasonal variability of the Asian summer monsoon, *Clim. Dyn*., 18, 85–102.

Awaka, J., T. Iguchi, and K. Okamoto (1997), Rain type classification algorithm for TRMM precipitation radar. *Proc. Int. Geoscience and Remote Sensing Symp*., Singapore, Institute of Electrical and Electronics Engineers, 4, 1633–1635.

Barros, A. P., and T. J. Lang (2003), Monitoring the monsoon in the Himalayas: observations in Central Nepal, June 2001, *Mon. Wea. Rev*., 131, 1408–1427.

Barros, A. P., G. Kim, E.Williams, and W. Nesbitt (2004), Probing orographic controls in the Himalayas during the monsoon using satellite imagery, *Nat. Hazards Earth Syst. Sci*., 4, 29–51.

Barros, A. P., M. Jhosi, J. Putkonen, and D. W. Burbank (2000), A study of 1999 monsoon rainfall in a mountainous region in Central Nepal using TRMM product and rain gauge observations, *Geophys. Res. Lett*., 27, 3683–3686.

Barros A. P., S. Chiao, T. J. Lang, D. Burbank, and J. Putkonen (2006), From weather to climate seasonal and interannual variability of storms and implications for errosion processes in the Himalaya, *Spec. Pap. Geol. Soc. Am*., 398, 17–18.

Barros, A. P., and T. J., Lang 1993, Dynamic modeling of the spatial distribution of precipitation in remote mountainous area, *Mon. Weather Rev., 121, 1195-1214.*

Bell, T. L., and P. K. Kundu (2000), Dependence of satellite sampling error on monthly averaged rain rates: comparison of simple models and recent studies, *J. Clim*., 13, 449–462.

Bhatta, B. C. (2005), Study on the seasonal and diurnal variation of the precipitation around the Himalayan region, Doctor thesis, Dep. of Earth and Environ, Sci., Nagoya Univ., Nagoya, Japan.

Bhatt, B. C., and K. Nakamura (2004), Characteristics of monsoon rainfall around the Himalayas revealed by TRMM precipitation radar, *Mon. Weather Rev*., 133, 149–165.

Bhatt, B. C., and K. Nakamura (2006), A climatological-dynamical analysis associated with precipitation around the southern part of the Himalayas, *J. Geophys. Res*, 111, doi: 10.1029/2005JD006197.

Bookhagen, B. (2010), Appearance of extreme monsoonal rainfall events and their impact on erosion in the Himalaya, *Geomat. Nat. Hazards Risk*, 1, 37–50.

Bookhagen, B., and D. W. Burbank (2006), Topography, relief, and TRMM-derived rainfall variations along the Himalaya, *Geophys. Res. Lett*., 33, L08405, doi:10.1029/2006GL026037.

Bookhagen, B., and D. W. Burbank (2010), Toward a complete Himalayan hydrological budget: Spatiotemporal distribution of snowmelt and rainfall and their impact on river discharge, *J. Geophys. Res*., 115, Fo3019, doi: 10.1029/2009JF001426.

Bookhagen, B., and M. R. Strecker (2008), Orographic barriers, high-resolution TRMM rainfall, and relief variations along the eastern Andes, *Geophys. Res. Lett*., 35, L06403, doi: 10.1029/2007GL032011.

Boos, W. R., and Z. Kuang (2010), Dominant control of the South Asian monsoon by orographic insulation versus plateau heating, *Nature*, 463, 218–222.

Chater, A. M., and A.P. Sturman (1998), Atmospheric conditions influencing the spillover of rainfall to lee of the southern Alps, New Zealand, *Int. J. Climatol*., 18, 77– 92.

Dairaku, K., S. Emori, and T. Oki (2004a), Rainfall amount, intensity, duration and frequency relationships in the Mae Cheam watershed in Southeast Asia, *J. Hydromet*., 5, 458–470.

Dairaku, K., S. Emori, and T. Oki (2004b), Observation and numerical experiments of Orographic precipitation in the Mae Chaem watershed in Southeast Asia CD-ROM Proceedings of The 6th International Study Confernce on GEWEX in Asia and GAME, GAME CD-ROM Publication No. 11, T2KD28Jul04173818 (reviewed).

Dhar, O. N., and P. R. Rakhecha (1981), The effect of elevation on monsoon rainfall distribution in the central Himalayas, *Monsoon Dynamics*, J., Lighthill, and R.P., Pearce, Eds., Cambridge Univ. Press, 253–260.

Dhar, O. N., M. K. Soman, and S. S. Mulye (1984), Rainfall over the southern slopes of the Himalayas and the adjoining plains during “breaks” in the monsoon, *J. Climatol*., 4, 671–676.

Engman, E. T., and D. M. Hersfield (1969), Precipitation climatology of the Sleepers River watershed near Denville, Vermount. Paper ARS, USDA, *Arg. Res. Ser*, pp. 41–148.

Flohn, H. (1957), Large-scale aspects of the "summer monsoon" in south and East Asia, J. *Meteorol. Soc. Jpn*, 75, 180–186.

Gadgil, S., and P. V. Joseph (2003), On breaks of the Indian monsoon, *proc. Indian Acad. Sci.*, 112, 529 –558.

Goswami, B. N., and R. S. Ajayahohan (2001), Intraseasonal oscillations and interannual variability of the Indian summer monsoon, *J. Clim.*, 14, 1180–1198.

Grossman R. L., and D. R. Durran, (1984), Interaction of low-level flow with the Western Ghats Mountains and offshore convection in the summer monsoon, Mon. Wea. Rev., 112, 652 – 672.

Higuchi, K., Y. Ageta, T. Yasunari, and J. Inoue (1982), Characteristics of precipitation during the monsoon season in high-mountain areas of the Nepal Himalaya, *Hydrol. Sci. J.*, 27, 251.

Houze, R. A., (2012), Orographic effects on precipitating clouds, *Rev. Geophys*., 50, RG1001.

Houze, A. R., D. C. Wilton and B. F. Smull (2007), Monsoon convection in the Himalayan region as seen by the TRMM precipitation radar, *Q. J. R. Meteorol. Soc*. 133, 1389–1411.

Huffman, G. J., et al. (2007), The TRMM multi-satellite precipitation analysis: Quasi-global, multi-year, combined-sensor precipitation estimates at fine scales, *J. Hydrometeorol*., 8, 38–55.

Krishnamurthy, V., and J. Shukla (2000), Intra-seasonal and inter-annual variations of rainfall over India, *J. Clim*., 13, 4366–4375.

Krishnan, R., C. Zhang, and M. Sugi (2000), Dynamics of breaks in the Indian summer monsoon, *J. Atmos. Sci*., 57, 1354–1372.

Kummerow, C., W. Barnes, T. Kozu, J. Shiue, and J Simpson (1998), The Tropical Rainfall Measuring Mission (TRMM) sensor package, *J. Atmos. Oceanic Technol*., 15, 809– 817.

Kummerow, C., et al. (2000), The status of Tropical Rainfall Measuring Mission (TRMM) after two years in orbit, *J. Appl. Meteorol*., 39, 1965–1982

Lang, T. J., and A. P. Barros (2002), An investigation of the onsets of the 1999 and 2000 monsoons in Central Nepal, *Mon. Weather Rev*., 130, 1299–1316.

Mani, A. (1981), *The climate of Himalaya, The Himalaya: Aspects of changes*, J. S. Lall and A. D. Moddie, Oxford Uni. Press, Delhi, 3–15.

Medina, S., R. A. Houze, A. Kumar, D. Niyogi (2010), Summer monsoon convection in the Himalayan region: Terrain and land cover effects, Q. J. R. Meteorol. Soc. 136, 593-616.

Nayava, J. L. (1980), Rainfall in Nepal. The Himalayan Review: *Nepal Geographical Soc*., 12, 1–18.

Nesbitt, S. W., and E. J. Zisper (2003), The diurnal cycle of rainfall and convective intensity according to three years of TRMM measurements, *J. Climate*, 16, 1456–1475.

Nesbitt, S. W., and A. M. Anders (2009), Very high resolution precipitation climatologies from the Tropical Rainfall Measuring Mission precipitation radar, *Geophys. Res. Lett*., 36, L15815, doi: 10.1029/2009GL038026.

Onogi, K., H. Koide, M. Sakamoto, S. Kobayashi, J. Tsutsui, H. Hatsushika, T. Matsumoto, N. Yamazaki, H. Kamahori, K. Takahashi, K. Kato, T. Ose, S. Kadokura, and K. Wada

2005: JRA-25: Japanese 25-year Re-analysis project–progress and status, *Quart. J. R. Meteorol. Soc*., 131, 3259–3268.

Rajeevan, M., S. Gadgil, and J. Bhate (2010), Active and break spells of the Indian summer monsoon, *J. Earth Syst. Sci*., 119, 229–247.

Ramamurhty, K. (1969), Monsoon of India: Some aspects of the "break" in the Indian southwest monsoon during July and August, *In Forcasting Manual*, 1–57 No. 18.3, Indian Meteorol. Dept., Poona India.

Rasmussen, K. L., and R. A. Houze (2011), Extreme summer convection in South America, J. Clim., 139, 2399–2420.

Romatschke, U., and R. A. Houze (2011a), Characteristics of precipitating convective systems in the South Asian monsoon, *J. Hydrometeorl*., 12, 157–180, doi: 10.1175/2010JHM1289.1.

Romatschke, U. and R. A. Houze (2011b), Characteristics of precipitating convective systems in the premonsoon season of South Asia, *J. Hydrometeorl*., 12, 3–26, doi: 10.1175/2010JHM1311.1.

Romatschke, U. and R. A. Houze (2010), Extreme summer convection in South America, *J. Climate*, 23, 3761-3791.

Romatschkke, U., S. Medina, and R. A. Houze (2010), Regional, seasonal, and diurnal variations of extreme convection in the south Asian region, *J. Climate, 23, 419–439.*

Rumley, J. B. (1965), An investigation of the distribution of rainfall with the elevation for selected station in Ecuador, M. Thesis, Texas A & M University, USA.

Shrestha, M. L. (2000), Interannual variation of summer monsoon rainfall over Nepal and its relation to southern oscillation index, *Meteorol. Atmos. Phys*., 75, 21–28.

Shrestha, D., P. Singh, and K. Nakamura (2012), Spatiotemporal variation of rainfall over the central Himalayan region revealed by precipitation radar, *J. Geophys. Res.*, doi:10.1029/2012JD018140.

Singh, P., and K. Nakamura (2010), Diurnal variation in summer monsoon precipitation during active and break periods over central India and southern Himalayan foothills, *J. Geophys. Res*., 115, doi:10.1029/2009JD012749, 2010.

Singh, P., and N. Kumar (1997), Effect of orography on precipitation in the western Himalayan region, *J. Hydrology*, 199, 183–206.

Singh, P., K. S. Ramasastri, and N. Kumar (1995), Topographical influence on precipitation distribution in different ranges of western Himalayas, *Nordic Hydrology* 26, 259–284.

Sokol, Z., and V. Bližňák (2009), Areal distribution and precipitation–altitude relationship of heavy short-term precipitation in the Czech Republic in the warm part of the year, *Atmos. Res*., 96, 652–662.

Steiner, M., R. A. Houze Jr., S. E. Yuter (1995), Climatological characterization of three-dimensional storm structure from operational radar and rain gauge data. *J. Appl. Meteor*., 34, 1978–2007.

Suprit, K., and D. Shankar (2008), Resolving orographic rainfall on the Indian West Coast, Int. *J. Climatol*., 28, 643–657.

Takahashi, H. G., H. Fujinami, T. Yasunari, and J. Matsumoto (2010), Diurnal rainfall pattern observed by Tropical Rainfall Measuring Mission Precipitation Radar (TRMM-PR)

around the Indochina peninsula, *J. Geophys. Res*., 115, D07109, doi:10.1029/2009JD012155.

Venkatesh, B., and M. K. Jose (2007), Identification of homogeneous rainfall regimes in parts of Western Ghats region of Karnataka, J. Earth Syst. Sci., 116, 321–329.

Webster, P. J., V. O. Magana, T. N. Palmer, J. Shukla, R. A. Tomas, M. Yanai, and T. Yasunari (1998), Monsoons: Process, predictability, and the prospects for prediction, *J. Geophys. Res*., 103, 14451–14510.

List of Figures

Figure 6. Variation of rainfall characteristics (rainfall, conditional rain rate, and rain frequency) with elevation for (a) pre-monsoon (MAM) and (b) summer monsoon (JJA). Solid, dotted, and dashed lines represent daily rainfall total (mm/day), conditional rain rate (mm/h), and frequency of rainfall (%), respectively.

Figure 7. Vertical structure of rainfall (mm/h) at 84.5°E for (a) pre-monsoon (MAM) and (b) summer monsoon (JJA). Dashed rectangle indicates cross section of study area over the southern slopes of the Himalayas. Gray line represents north-south Himalayan topography at the same location.

Figure 8. Horizontal distribution of rainfall types during summer monsoon (JJA). (a) Difference between the convective and stratiform rain rates (mm/h), and (b) difference between the occurrence of stratiform and convective rainfall events. The area enclosed by the black oval lines represents the central Himalayan region (CHR).

Figure 9. Altitudinal variation in rain type during summer monsoon (JJA) for (a) occurrence of rain events (pixel) and (b) rain rate (mm/h). Solid and dashed lines indicate stratiform rainfall and convective rainfall, respectively.

Figure 10. As in Fig. 12, but for (a) and (b) active monsoon, and (c) and (d) break monsoon.

Figure 11. Altitudinal variation in rain characteristics during active (dashed line) and break (solid line) periods for (a) rain total (mm/day), (b) active/break rain percentage (%), (c) rain-conditioned rain rate (mm/h), and (d) frequency of rain (%).

Figure 12. Horizontal patterns of equivalent potential temperature (K; color shaded), winds (m/s; black arrows), and specific humidity (g/kg, black contours) at 925 hPa for (a) JJA

climatological mean and (c) MAM case study. Difference in equivalent potential temperature between two pressure levels (925 and 600 hPa) for (b) JJA climatological mean and (d) MAM case study. Gray shading represents topography above 800 m (~925 hPa).

Figure 13. As in Fig. 12, but for (a) active monsoon, and (b) break monsoon.

Figure 14. Horizontal distribution of rain characteristics over the Western Ghats (WG, left panel of each figure) and Myanmar west coast (MWC, right panel of each figure) region: (a) rain rate, (b) rain frequency, (c) conditional rain rate, and (d) storm height. Contour line represents 500 m elevations.

Figure 15. Two sample profiles from west to east of the Western Ghats (a) and Myanmar west coast (b). Heavy solid, thin solid, grey, and dashed lines represent topography (m), daily rainfall total (mm/d), rain frequency (%), and conditional rain rate (mm/h), respectively.

Figure 16. Difference between the convective and stratiform rain amounts for (a) Western Ghats (WG), and (b) Myanmar west coast (MWC). Orographic contour are as in Fig. 2.

Figure 17. Distribution of rain characteristics over the Western Ghats (WG, left panel of each figure) and Myanmar west coast (MWC, right panel of each figure) region: (a) stratiform rain frequency, (b) convective rain frequency. Orographic contour are as in Fig. 2.

Figure 18. Vertical profile of conditional rain rates over specific region: (a) Western Ghats, (b) Myanmar west coast, and (c) central Himalayas.

Figure 19. Vertical cross-section of rain rate over the Western Ghats (WG, at 15°N) (a) and over the Myanmar west coast (MWC, 18.5°N) (b). Black line represents east-west topography of coastal mountain ranges.

Figure 20. Horizontal distribution of rain characteristics around the Andes: (a) rain rate (mm/d), (b) rain frequency (%), (c) conditional rain rate (mm/h), and (d) storm-top height (m). Contour lines represent 500 and 3000 m elevations.

Figure 21. Variation of rainfall characteristics with elevation for (a) Central Andes (CA) and (b) Southern Andes (SA). Solid, dotted, and dashed lines represent daily rainfall total (mm/d), conditional rain rate (mm/h), and frequency of rainfall (%).

Figure 22. Horizontal distribution of stratiform rain frequency (left panel) and conditional rain rate of convective rain (right panel). Orographic contour are as in Fig. 8.

Figure 23. As in figure 6, but for Central Andes (a) and Southern Andes (b). Each region is divided into two subregions: higher terrain (>500 m) and lower terrain (<500 m).

Figure 24. As in figure 7, but for Central Andes (a) and Southern Andes (b).

Figure 25. JRA-25 climatology of equivalent potential temperature (K; color shaded), winds (m/s; black arrows), and specific humidity (g/kg, black contours) at 925 hPa (a), and difference in equivalent potential temperature between two pressure levels (925 and 600 hPa) (b), for South American summer (December–February). Gray shading represents topography above 800 m (~925 hPa).

Figure 26. Schematic illustrations of spatiotemporal variation in rainfall for (a) pre-monsoon (MAM), (b) summer monsoon (JJA), (c) active monsoon, and (d) break monsoon.